



# A nitrate ion chemical-ionization atmospheric-pressure-interface time-of-flight mass spectrometer ( $\text{NO}_3^-$ ToFCIMS) sensitivity study

Stéphanie Alage<sup>1</sup>, Vincent Michoud<sup>2</sup>, Sergio Harb<sup>1</sup>, Bénédicte Picquet-Varrault<sup>1</sup>, Manuela Cirtog<sup>1</sup>, Avinash Kumar<sup>3</sup>, Matti Rissanen<sup>3,4</sup>, and Christopher Cantrell<sup>1</sup>

<sup>1</sup>LISA, Université Paris-Est Créteil and Université Paris Cité, CNRS, 94010 Créteil, France

<sup>2</sup>LISA, Université Paris Cité and Université Paris-Est Créteil, CNRS, 75013 Paris, France

<sup>3</sup>Aerosol Physics Laboratory, Physics Unit, Faculty of Engineering and Natural Sciences, Tampere University, 33720 Tampere, Finland

<sup>4</sup>Department of Chemistry, University of Helsinki, 00014 Helsinki, Finland

**Correspondence:** Vincent Michoud (vincent.michoud@lisa.ipsl.fr)

Received: 14 February 2024 – Discussion started: 20 February 2024

Revised: 11 June 2024 – Accepted: 17 June 2024 – Published: 13 August 2024

**Abstract.** Volatile organic compounds (VOCs) play a key role in tropospheric chemistry, giving rise to secondary products such as highly oxygenated organic molecules (HOMs) and secondary organic aerosols (SOAs). HOMs, a group of low-volatility gas-phase products, are formed through the autoxidation process of peroxy radicals ( $\text{RO}_2$ ) originating from the oxidation of VOCs. The measurement of HOMs is made by a  $\text{NO}_3^-$  ToFCIMS instrument, which also detects other species like small highly oxygenated VOCs (e.g., dicarboxylic acids) and sulfuric acid ( $\text{H}_2\text{SO}_4$ ). The instrument response to HOMs is typically estimated using  $\text{H}_2\text{SO}_4$ , as HOMs are neither commercially available nor easily synthesized in the laboratory. The resulting calibration factor is then applied to quantify all species detected using this technique. In this study, we explore the sensitivity of the instrument to commercially available small organic compounds, primarily dicarboxylic acids, given the limitations associated with producing known amounts of HOMs for calibration. We compare these single-compound calibration factors to the one obtained for  $\text{H}_2\text{SO}_4$  under identical operational conditions. The study found that the sensitivity of the  $\text{NO}_3^-$  ToFCIMS varies depending on the specific type of organic compound, illustrating how a single calibration factor derived from sulfuric acid is clearly inadequate for quantifying all detected species using this technique. The results highlighted substantial variability in the calibration factors for the tested organic compounds, with 4-nitrocatechol exhibiting the highest sensitivity and pyruvic acid the lowest. The obtained sulfuric

acid calibration factor agreed well with the previous values from the literature. In summary, this research emphasized the need to develop reliable and precise calibration methods for progressively oxygenated reaction products measured with a  $\text{NO}_3^-$  chemical-ionization mass spectrometer (CIMS), for example, HOMs.

## 1 Introduction

Volatile organic compounds (VOCs), originating from both natural sources (such as land or marine ecosystems, also known as biogenic VOCs or BVOCs) and human-made sources (referred to as anthropogenic VOCs or AVOCs), play crucial roles in tropospheric chemistry. Once released into the atmosphere, VOCs undergo chemical oxidation reactions initiated primarily by the three main atmospheric oxidants: hydroxyl radicals ( $\text{OH}\cdot$ ), nitrate radicals ( $\text{NO}_3\cdot$ ), and ozone ( $\text{O}_3$ ) (Finlayson-Pitts, 2010). Such chemical reactions ultimately result in the production of carbon dioxide ( $\text{CO}_2$ ) but also may lead to the formation of multifunctional organic compounds, although this is a minor pathway. These are typically less volatile than the initial compounds, except in cases of fragmentation, and can therefore take part in the formation of secondary organic aerosol (SOA) (Kanakidou et al., 2005; Riipinen et al., 2011). Consequently, VOCs are well recognized as important precursors for the formation and growth

of SOA as well as other secondary products, such as ground-level ozone, which significantly impact air quality, human health, and climate (Seinfeld and Pandis, 2016).

Recently, studies have revealed that AVOCs and BVOCs play crucial roles as key precursors in the gas-phase formation of highly oxygenated organic molecules (HOMs). Initially labeled as extremely-low-volatility organic compounds (ELVOCs) to emphasize their pivotal role in particle formation and growth (Schobesberger et al., 2013; Ehn et al., 2012, 2014; Jokinen et al., 2015), it has since been suggested that these compounds span a broader range of volatility classes (Kurtén et al., 2016), including ULVOCs (ultra-low-volatility organic compounds), ELVOCs, LVOCs (low-volatility organic compounds), and SVOCs (semi-volatile organic compounds). This recognition acknowledges their ability to contribute to gas-to-particle partitioning with varying levels of efficiency (Donahue et al., 2011; Kirkby et al., 2016; Tröstl et al., 2016; Bianchi et al., 2019; Guo et al., 2022b).

The term “HOMs” primarily refers to a class of products generated through the gas-phase chemical process known as autoxidation (Bianchi et al., 2019; Berndt et al., 2021). The significance of autoxidation in atmospheric chemistry only gained recognition in the past decade (Crouse et al., 2013; Ehn et al., 2014; Rissanen et al., 2014). Overall, it is characterized by an intramolecular H-atom shift within peroxy radicals (RO<sub>2</sub>•), which are formed following the initial reaction of VOCs with oxidants, yielding a hydroperoxide functionality (HOO–). This is followed by rapid addition of O<sub>2</sub> to form a new, more oxygenated RO<sub>2</sub>•. This process can repeat multiple times (Crouse et al., 2013; Ehn et al., 2017; Møller et al., 2019; Vereecken and Nozière, 2020). Autoxidation may also be interrupted at each stage by classical termination reactions (unimolecular or bimolecular reactions). This evolution depends largely on the chemical environment. These reactions convert HOM-RO<sub>2</sub>• into closed-shell molecules, while preserving the number of carbon atoms. In some instances, this interruption can lead to the formation of RO• radicals, which subsequently contribute to the production of closed-shell molecules. Due to their low volatility, HOMs are expected to efficiently partition into the particle phase. Consequently, they have the potential to condense onto existing aerosols or contribute to new particle formation (NPF) (Ehn et al., 2014; Riccobono et al., 2014; Kirkby et al., 2016).

Following their initial observation in the atmosphere as ambient ion clusters with the nitrate ion (NO<sub>3</sub><sup>-</sup>), nitrate chemical-ionization time-of-flight mass spectrometry (NO<sub>3</sub><sup>-</sup> ToFCIMS) was employed to detect neutral HOMs in the atmosphere and in laboratory settings (Ehn et al., 2012; Jokinen et al., 2014). Other reagent ions for detecting HOMs, such as acetate and iodide, have also been used (e.g., Berndt et al., 2016; Iyer et al., 2017; Hansel et al., 2018; Riva et al., 2019).

The nitrate-ion-based chemical-ionization atmospheric-pressure-interface time-of-flight mass spectrometer (NO<sub>3</sub><sup>-</sup> ToFCIMS; Aerodyne Research Inc. and ToFwerk AG) is the

key online mass spectrometry (MS) instrument characterized for organic compound detection in this study. This instrument is capable of measuring gas-phase non-radical HOMs, highly oxidized peroxy radicals (HOM-RO<sub>2</sub>•), certain oxygenated VOCs (OVOCs, such as small dicarboxylic acids), and sulfuric acid (H<sub>2</sub>SO<sub>4</sub>) with high resolution and sensitivity (Bianchi et al., 2019; Ehn et al., 2017; Rissanen, 2021). A concise description of the instrument's principles and the operational parameters used are provided in the following section.

Calibrating the NO<sub>3</sub><sup>-</sup> ToFCIMS is essential to determine the appropriate calibration coefficient, C<sub>X</sub>, which reflects a specific instrument's detection sensitivity to an organic compound, denoted as X, and can be used to determine the molecule's concentration [X]. It is important to note that it is almost certainly impossible to derive a single calibration factor capable of evaluating all possible organic compounds. The NO<sub>3</sub><sup>-</sup> ToFCIMS can detect a broad range of low-volatility multifunctional organic species, and finding suitable oxygenated organic molecule standards for calibration is challenging, especially considering the complexity and limited knowledge of HOMs' precise structures. To determine the appropriate C<sub>X</sub> values, a series of known concentrations of a compound must be sampled. The C<sub>X</sub> value is then obtained as the slope of the plot illustrating the known concentration as a function of the normalized ion product signals.

In this paper, we tested several commercially available organic compounds as potential direct calibrants for the NO<sub>3</sub><sup>-</sup> ToFCIMS instrument. We describe and discuss the implementation of two calibration approaches in Sect. 2.2.1 and 2.2.2. Additionally, we established a method to experimentally determine the vapor pressure (P<sub>vap</sub>) of specific solid organic compounds, including malonic acid, detailed in Sect. 2.2.2. Finally, we discuss instrument calibration using sulfuric acid and compare the results to those obtained with organic compounds.

## 2 Materials and experimental methods

### 2.1 The nitrate ToFCIMS

#### 2.1.1 Principle

The NO<sub>3</sub><sup>-</sup> ToFCIMS used in this study is composed of two primary components: the chemical-ionization (CI) inlet (Eisele and Tanner, 1993; Jokinen et al., 2012) and the atmospheric-pressure-interface time-of-flight mass spectrometer (APi-ToFMS) (Junninen et al., 2010). Briefly, nitrate reagent ions (HNO<sub>3</sub>)<sub>n=0–2</sub> · NO<sub>3</sub><sup>-</sup> are generated by passing a 30 sccm (standard cubic centimeters per minute) stream of dry air through a small amount (2–20 mL) of liquid nitric acid (HNO<sub>3</sub>) placed in a glass vial producing a mixture of gas-phase HNO<sub>3</sub> in air (about 6 % vol). This flow is mixed with the sheath flow and then exposed to soft X-ray radi-

ation (Hamamatsu photoionizer model C12646 power supply; model L9491 source head 9.5 keV), resulting in high-density ion production. Subsequently, electrostatic voltages are applied to the drift tube to guide the reagent ions toward the center axis of the inlet, allowing them to interact with neutral molecules in the sample gas flow with a reaction time of approximately 300 ms. The sample gas is introduced into the center axis of the CI inlet through a 3/4 in. (19.05 mm) stainless-steel tube at a flow rate of around  $6 \text{ L min}^{-1}$  (liter per minute). Ion–molecule reactions with  $\text{NO}_3^-$  can occur through either proton abstraction and clustering (e.g., small dicarboxylic acids) or only by clustering (e.g., OVOCs, HOMs) (Field, 1968; Jokinen et al., 2012). Clustering reactions involve a sample molecule such as HOMs that generates a stable ion–molecule cluster  $(\text{NO}_3) \cdot \text{HX}^-$  (Hytinen et al., 2015). The product and reagent ions then enter the mass spectrometer through a critical orifice (diameter 0.3 mm), at a flow of approximately  $0.8 \text{ L min}^{-1}$ , and are subsequently focused through a series of ion optics as they move towards the time-of-flight mass spectrometer (ToFMS) region where they are separated and detected according to their time of flight in the ToF chamber. The time of flight is then processed and converted to the mass-to-charge ratio of the ion in question. The instrument is characterized by a moderate mass resolution of about  $3700m / \Delta m$ . The ToFMS is operated at 16.7 kHz frequency with a  $60 \mu\text{s}$  ToF extraction period. The mass spectrum range is 7–1126 Th. Data are collected at a 1 s time resolution and averaged over 1 min intervals. The mass ( $m/z$ ) calibration, a crucial step in data processing, is usually performed with respect to calibrant peaks. Typically, the three reagent ion peaks,  $\text{NO}_3^-$ ,  $(\text{HNO}_3) \cdot \text{NO}_3^-$ , and  $(\text{HNO}_3)_2 \cdot \text{NO}_3^-$  ( $m/z = 61.99, 124.98, \text{ and } 187.98$ , respectively) are used. However, it is important to have several reference peaks well distributed along the covered  $m/z$  range. Fluorinated organic compounds appeared clearly as contaminants that likely originated from Teflon<sup>®</sup> sampling lines used in early experiments and therefore appeared in the mass spectra. This phenomenon is well known in the use of  $\text{NO}_3^-$  ToFCIMS (Ehn et al., 2012). To make use of this, several perfluorinated organic acids covering the upper  $m/z$  range were added continuously to the instrument (see Table 1), so that the mass calibration could cover a wider mass range, leading to an improvement of the mass calibration with a mass accuracy of less than 10 ppm.

### 2.1.2 Calibration methods

For the quantification of HOMs, as well as other organic compounds detected by the ToFCIMS, under typical sampling conditions, the following general Eq. (1) is employed:

$$[\text{X}] = C_X \times \frac{i_{\text{X}^-} + \sum_{n=0-2} i_{\text{HX}(\text{HNO}_3)_n\text{NO}_3^-}}{i_{\text{NO}_3^-} + i_{(\text{HNO}_3)\text{NO}_3^-} + i_{(\text{HNO}_3)_2\text{NO}_3^-} + i_{(\text{H}_2\text{O})\text{NO}_3^-}}, \quad (1)$$

where  $C_X$  is the calibration coefficient ( $\text{molec. cm}^{-3} \text{ ncps}^{-1}$ ); ncps: normalized counts per second;  $[\text{X}]$  is the concentration

of the measured compound by the ToFCIMS;  $i_{\text{X}^-}$  is the ion signal of the deprotonated product ion (typically for acidic organic compounds);  $\sum_{n=0-2} i_{\text{HX}(\text{HNO}_3)_n\text{NO}_3^-}$  is the sum of the product ion cluster signals; and  $i_{\text{NO}_3^-} + i_{(\text{HNO}_3)\text{NO}_3^-} + i_{(\text{HNO}_3)_2\text{NO}_3^-} + i_{(\text{H}_2\text{O})\text{NO}_3^-}$  is the sum of reagent ion signals for  $\text{NO}_3^-$ ,  $(\text{HNO}_3) \cdot \text{NO}_3^-$ ,  $(\text{HNO}_3)_2 \cdot \text{NO}_3^-$ , and  $\text{H}_2\text{O} \cdot \text{NO}_3^-$ .

The presence of  $\text{H}_2\text{O} \cdot \text{NO}_3^-$  clusters was identified in the mass spectra, and their response showed variations with changing humidity conditions during sampling. Consequently, their signals were incorporated into the calculations using Eq. (1), although their influence was found to be relatively minor, typically accounting for 0.1 %–2 % of the total reagent ion signal.

The most commonly employed method in the literature relies on using sulfuric acid as a calibrant, assuming that it exhibits the same ionization kinetic rate constant and comparable transmission efficiency as HOMs (Ehn et al., 2014; Kirkby et al., 2016). Employing a  $C_X$  value determined for  $\text{H}_2\text{SO}_4$  introduces considerable uncertainty into the obtained values. In brief, calibrations using sulfuric acid are typically conducted by generating a known quantity of  $\text{OH} \cdot$  in an excess of  $\text{SO}_2$ , leading to a known amount of gas-phase sulfuric acid (Berndt et al., 2014). Most studies are based on a dedicated setup developed to calibrate a  $\text{NO}_3^-$  chemical-ionization mass spectrometer (CIMS) with  $\text{H}_2\text{SO}_4$ . This system was estimated to give an overall uncertainty of around 33 % (Eisele and Tanner, 1993; Kürten et al., 2012). Furthermore, Jokinen et al. (2012) presented  $C_X$  values obtained by comparing  $\text{H}_2\text{SO}_4$  measured in ambient air by a ToFCIMS to concentrations measured by a calibrated quadrupole CIMS. Other direct calibrations have been reported in the literature, using alternative organic compounds such as perfluorinated heptanoic acid  $\text{C}_7\text{HF}_{13}\text{O}_2$  (Ehn et al., 2014), malonic acid  $\text{C}_3\text{H}_4\text{O}_4$  (Krechmer et al., 2015; Isaacman-VanWertz et al., 2018; Massoli et al., 2018), and 4-nitrophenol  $\text{C}_6\text{H}_5\text{NO}_3$  (Cheng et al., 2021). It is noteworthy that many studies use previously determined  $C_X$  values from the literature introducing potentially larger uncertainties into their measurements (Zha et al., 2018; Wang et al., 2020; Garmash et al., 2020; Meder et al., 2023; Zhang et al., 2022). Despite being obtained under varying experimental conditions, the reported calibration factors generally exhibit a similar order of magnitude in the range of  $(0.2\text{--}6) \times 10^{10} \text{ molec. cm}^{-3} \text{ ncps}^{-1}$  (Table 2).

## 2.2 Experimental approaches

### 2.2.1 Approach 1 – organic vapor pressure quantification

Following approach 1, organic compounds (OCs) that are in the form of solid powders (liquid form for pyruvic acid) are placed in 1/4 in. (6.35 mm) outside diameter stainless-steel tubes. The compounds are confined by filters, composed of stainless-steel grids or glass wool, on each end that serve to

**Table 1.** List of perfluorinated organic compounds chosen for mass calibration covering a wide range of  $m/z$ .

Compound	MW (g mol <sup>-1</sup> )	Chemical formula	Form of detection ( $m/z$ of detection)
Perfluoropropionic acid	164.03	C <sub>2</sub> F <sub>5</sub> COOH	C <sub>3</sub> HF <sub>5</sub> O <sub>2</sub> · (NO <sub>3</sub> ) <sup>-</sup> (225.978) > C <sub>3</sub> F <sub>5</sub> O <sub>2</sub> <sup>-</sup> (162.982)
2,3,4,5,6-Pentafluorobenzoic acid	212.07	C <sub>6</sub> F <sub>5</sub> COOH	C <sub>7</sub> HF <sub>5</sub> O <sub>2</sub> · (NO <sub>3</sub> ) <sup>-</sup> (274.058) >> C <sub>7</sub> F <sub>5</sub> O <sub>2</sub> <sup>-</sup> (211.07)
Perfluoroheptanoic acid	364.06	C <sub>6</sub> F <sub>13</sub> COOH	C <sub>7</sub> HF <sub>13</sub> O <sub>2</sub> · (NO <sub>3</sub> ) <sup>-</sup> (426.048) > C <sub>7</sub> F <sub>13</sub> O <sub>2</sub> <sup>-</sup> (363.06)
Perfluorononanoic acid	464.08	C <sub>8</sub> F <sub>17</sub> COOH	C <sub>9</sub> HF <sub>17</sub> O <sub>2</sub> · (NO <sub>3</sub> ) <sup>-</sup> (526.068) > C <sub>9</sub> F <sub>17</sub> O <sub>2</sub> <sup>-</sup> (463.08)
Perfluoroundecanoic acid	564.09	C <sub>10</sub> F <sub>21</sub> COOH	C <sub>11</sub> HF <sub>21</sub> O <sub>2</sub> · (NO <sub>3</sub> ) <sup>-</sup> (626.068) >> C <sub>11</sub> F <sub>21</sub> O <sub>2</sub> <sup>-</sup> (563.09)

>: slightly higher than; >>: significantly higher than.

**Table 2.** Calibration factors from the literature using NO<sub>3</sub><sup>-</sup> ToFCIMS instruments.

Reference	Calibration coefficient (molec. cm <sup>-3</sup> ncps <sup>-1</sup> )	Calibrant
Jokinen et al. (2012)	5 × 10 <sup>9</sup> ; 1.89 × 10 <sup>10</sup>	H <sub>2</sub> SO <sub>4</sub>
Rissanen et al. (2014)	1.94 × 10 <sup>10</sup>	H <sub>2</sub> SO <sub>4</sub>
Berndt et al. (2015, 2016), Jokinen et al. (2014, 2015)	1.85 × 10 <sup>9</sup>	H <sub>2</sub> SO <sub>4</sub>
Mutzel et al. (2015)	8.4 × 10 <sup>9</sup>	H <sub>2</sub> SO <sub>4</sub>
Kirkby et al. (2016)	6.5 × 10 <sup>9</sup>	H <sub>2</sub> SO <sub>4</sub>
Kürten et al. (2016)	6 × 10 <sup>9</sup>	H <sub>2</sub> SO <sub>4</sub>
Riva (2019)	2 × 10 <sup>10</sup>	H <sub>2</sub> SO <sub>4</sub>
Quéléver et al. (2019)	1.65 × 10 <sup>9</sup>	H <sub>2</sub> SO <sub>4</sub>
Pullinen et al. (2020)	3.7 × 10 <sup>10</sup>	H <sub>2</sub> SO <sub>4</sub>
Shen et al. (2021) Zhao et al. (2021) Guo et al. (2022a) Luo et al. (2023)	2.5 × 10 <sup>10</sup>	H <sub>2</sub> SO <sub>4</sub>
Cheng et al. (2021)	1.66 × 10 <sup>10</sup>	H <sub>2</sub> SO <sub>4</sub>
Xu et al. (2021)	1.57 × 10 <sup>10</sup> ; 2 × 10 <sup>10</sup>	H <sub>2</sub> SO <sub>4</sub>
Dam et al. (2022)	6 × 10 <sup>10</sup>	H <sub>2</sub> SO <sub>4</sub>
Wang et al. (2022)	1.1 × 10 <sup>10</sup>	H <sub>2</sub> SO <sub>4</sub>
Ehn et al. (2014)	1.6 × 10 <sup>10</sup>	C <sub>7</sub> HF <sub>13</sub> O <sub>2</sub>
Krechmer et al. (2015) Massoli et al. (2018)	7.9 × 10 <sup>10</sup>	C <sub>3</sub> H <sub>4</sub> O <sub>4</sub>
Cheng et al. (2021)	1.62 × 10 <sup>10</sup>	4-nitrophenol

keep solid–liquid materials from entering the instrument (see Fig. 1). This device is designated as the source tube (ST) and is heated using temperature-controlled heating set to a fixed temperature whose value was chosen depending on the compound (ranging from 20 to 90 °C). Heating serves to increase the vapor pressure of the compound. The choice of temperature varies with the compound being studied and is determined through experimental testing. These tests involve gradually increasing the temperature while measuring with

the instrument, as well as avoiding the decomposition of the compound. It was observed that the signals from the reagent ions began to diminish beyond a certain temperature, both in the presence and absence of a sample. This somewhat restricted the range of compounds that could be employed with this method.

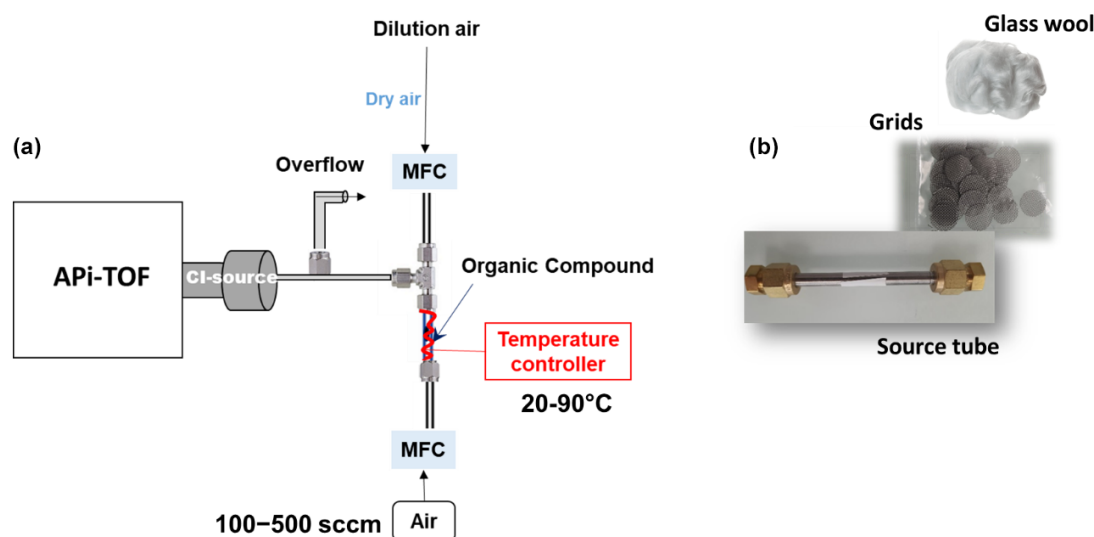
The vaporized compounds are transferred out of the ST by a regulated flow of synthetic air (100 to 500 sccm) controlled by a calibrated mass flow controller (MFC). The flow is diluted by additional dry zero air that controls the final concentration and provides excess flow to the inlet (see Fig. 1a).

Table 3 provides a summary of the tested organic compound calibrants for the NO<sub>3</sub><sup>-</sup> ToFCIMS, consisting mainly of dicarboxylic acids. Additional compounds were tested and were not detected by the instrument. This could possibly be due to either the instrument's lack of sensitivity towards them or the need to develop more sophisticated methods to generate gas-phase standard mixtures of low-volatility compounds. It is also possible that higher heating temperatures could be required to generate them in the gaseous phase, but we found that the maximum temperatures that could be used without changing the instrument's performance limited the further increase in the source tube temperatures. The instrument exhibited a measurable response to the following organic compounds: propanoic (PrA, purity 99.5 %), pyruvic (PyA), lactic (LA), oxalic (OxA, purity ≥ 99.0 %), succinic (SucA, purity ≥ 99.5 %), tartaric (TA, purity ≥ 99.0 %), and malonic (MA, purity ≥ 99.0 %) acids, along with 4-nitrocatechol (4-NC, purity ≥ 96 %) (the only nitrophenol tested).

The concentrations of these compounds that were produced and injected into the ToFCIMS were calculated using Eq. (2).

$$[\text{OC}] (\text{ppbv}) = \frac{F_{\text{OC}} (\text{sscm}) \times P_{\text{vap}} (\text{Pa})}{(F_{\text{OC}} (\text{sscm}) + F_{\text{diluent}} (\text{sscm})) \times P_{\text{atm}} (\text{Pa})} \times 10^9, \quad (2)$$

where [OC] is the concentration of the organic compound in parts per billion by volume (ppbv),  $F_{\text{OC}}$  is the flow through the ST in standard cubic centimeters per minute (sccm),  $P_{\text{vap}}$  is the vapor pressure of the organic compound in pascal (Pa)



**Figure 1.** (a) Experimental setup used for  $\text{NO}_3^-$  ToFCIMS calibration using organic vapor pressure quantification. (b) Stainless-steel grids, glass wool, and tube containing the organic compound.

**Table 3.** Candidate organic compounds used to evaluate the sensitivity of the instrument.

Compound	MW ( $\text{g mol}^{-1}$ )	Chemical structure
Propanoic acid	74.08	$\text{C}_3\text{H}_6\text{O}_2$
Pyruvic acid	88.06	$\text{C}_3\text{H}_4\text{O}_3$
Oxalic acid	90.03	$\text{C}_2\text{H}_2\text{O}_4$
Lactic acid	90.08	$\text{C}_3\text{H}_6\text{O}_3$
Malonic acid	104.06	$\text{C}_3\text{H}_4\text{O}_4$
Succinic acid	118.09	$\text{C}_4\text{H}_6\text{O}_4$
Tartaric acid	150.08	$\text{C}_4\text{H}_6\text{O}_6$
4-Nitrocatechol	155.11	$\text{C}_6\text{H}_5\text{NO}_4$
Benzenesulfonic acid*	158.17	$\text{C}_6\text{H}_6\text{O}_3\text{S}$

\* Upon heating, this compound exhibits color changes, indicating decomposition.

at the ST temperature employed,  $F_{\text{diluent}}$  is the dilution flow in sccm, and  $P_{\text{atm}}$  is the ambient pressure in pascal (Pa).

The overall formula is multiplied by  $10^9$  to convert the mixing ratio to ppbv. For these experiments, vapor pressures are either obtained experimentally (see Sect. 2.2.2) or extracted from the literature.

The  $P_{\text{vap}}$  of a compound at a specific temperature  $T_2$  was calculated using the Clausius–Clapeyron equation (Eq. 3) by using a known value of the  $P_{\text{vap}}$  at a reference temperature,  $T_1$ , and either the enthalpy of vaporization for a liquid or the enthalpy of sublimation for a solid compound, as appropriate.

$$\ln\left(\frac{P_2}{P_1}\right) = \frac{\Delta H_{\text{vap/sub}}}{R} \times \left(\frac{1}{T_1} - \frac{1}{T_2}\right), \quad (3)$$

where  $P_1$  and  $P_2$  are the vapor pressures at temperatures  $T_1$  and  $T_2$ , respectively;  $\Delta H_{\text{vap/sub}}$  is the enthalpy

of vaporization or sublimation; and  $R$  is the gas constant ( $8.314 \text{ J mol}^{-1} \text{ K}^{-1}$ ).

## 2.2.2 Experimental determination of vapor pressure of malonic acid

A series of laboratory experiments was conducted to experimentally determine the vapor pressure ( $P_{\text{vap}}$ ) of MA, which is a solid at room temperature. The experimental procedure was as follows.

1. Air at a flow rate of 300 sccm was passed through the ST, which was heated to  $50^\circ\text{C}$  and connected to the ToFCIMS instrument.
2. The experiment was left to run for a duration of 1 week or longer, enabling the measurement of a detectable loss of mass using an analytical balance with an accuracy of 0.1 mg.
3. The vapor pressure of the compound was then deduced using Eq. (4), which is derived from the ideal gas law. This experimental procedure was repeated three times for accuracy and consistency.

$$P_{\text{vap}} = \frac{\Delta m_{\text{meas}}(\text{g}) \times R \times T(\text{K})}{\text{MW}(\text{g mol}^{-1}) \times V(\text{L})}, \quad (4)$$

where  $P_{\text{vap}}$  is the vapor pressure in atmospheres (atm),  $\Delta m_{\text{meas}}$  is the weight loss (g),  $T$  is the temperature (K),  $V$  is the volume of air (L) found by multiplying the air-flow rate over the source tube ( $\text{L min}^{-1}$ ) by the time (min), and  $R = 0.082057 \text{ L atm mol}^{-1} \text{ K}^{-1}$ .

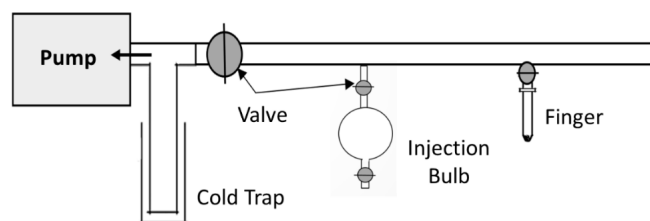


**Figure 2.** Vacuum line for the preparation of the compounds injected into the simulation chamber.

### 2.2.3 Approach 2 – organic sensitivity by FTIR quantification

The experimental methodology of approach 2 consists of the two main elements:

- the atmospheric simulation chamber (CSA) equipped with an in situ FTIR (Fourier transform infrared) spectrometer instrument (Bruker Vertex 80);
- a vacuum line coupled to a bulb of known volume (0.3 L), which was used (see Fig. 2) to prepare gaseous OCs from liquid standards to inject into the chamber.

Briefly, the CSA chamber (LISA, Université Paris-Est Créteil) is an atmospheric simulation chamber, which is a cylindrical Pyrex reactor (volume: 977 L; length: 6 m; diameter: 45 cm) designed for investigating atmospheric gas processes under controlled conditions. In addition, it is equipped with instrumentation for analysis using ultraviolet–visible and infrared spectroscopy (Doussin et al., 1997; Picquet-Varrault et al., 2005). The chamber is equipped with an efficient homogenization system, ensuring a mixing time of less than 1 min. In our experimental studies, FTIR spectra were averaged for 5 min and covered the spectral range of 500–4000  $\text{cm}^{-1}$ , with a spectral resolution of 0.5  $\text{cm}^{-1}$  and an optical path length of 214 m.

The basic principle of the vacuum line involves placing the compound in a glass finger connected to the vacuum line, which is plunged into a cold trap of liquid nitrogen. The vacuum is then applied to eliminate air and volatile impurities. The pump is then isolated, and the finger is brought back to room temperature, allowing the evaporation of the compound into the bulb. The bulb pressure is measured, and the concentration of the compound is calculated using Eq. (5).

$$[\text{OC}] (\text{ppbv}) = \frac{(P_{f,\text{bulb}} - P_{i,\text{bulb}}) \times V_{\text{bulb}}}{P_{\text{CSA}} \times V_{\text{CSA}}} \times 10^9, \quad (5)$$

where  $P_{i,\text{bulb}}$  is the initial bulb pressure (limit vacuum around  $10^{-4}$  mbar),  $P_{f,\text{bulb}}$  is the final bulb pressure,  $P_{\text{CSA}}$  is the CSA chamber pressure, and  $V_{\text{bulb}}$  and  $V_{\text{CSA}}$  are the bulb and CSA chamber volumes, respectively.

The principle of this approach (see Fig. 3) involves several steps, as follows:

1. the CSA is first filled with nitrogen gas to slightly exceed ambient pressure by about 5 mbar;
2. the liquid organic under study is introduced into the chamber by passing synthetic air through the bulb;
3. FTIR spectra are recorded, and the stabilization of the corresponding organic signal is ensured;
4. the chamber contents are diluted using a pumping system and by connecting the  $\text{NO}_3^-$  ToFCIMS to the chamber, using a heated 1/4 in. diameter stainless-steel line (maintained at  $\sim 40^\circ\text{C}$ ), yielding a total dilution flow of approximately 23  $\text{L min}^{-1}$ ;
5. the pressure inside the chamber is maintained by continuously introducing  $\text{N}_2$  into the chamber;
6. the normalized ion counts of the OC, obtained by the  $\text{NO}_3^-$  ToFCIMS, and the chamber concentrations derived from the FTIR (using the reference IR spectrum for the OC) are used to determine a calibration factor for the compound being studied.

This approach was only appropriate for our liquid compounds that are characterized by higher vapor pressures compared to the solid ones and can be introduced in sufficient quantities to compensate for rather high detection limits of the FTIR.

The FTIR spectra were processed using analysis of infrared spectra (ANIR) software, which consists of a classic fitting routine of the spectra. For that, the reference spectrum of the compound in question must be available with the known optical path,  $L$  (cm); reference concentration of the absorbing species,  $C$  ( $\text{molec. cm}^{-3}$ ); and thus the effective absorption cross sections as a function of wavelength or wavenumber,  $\varepsilon$  ( $\lambda$ ).

The total uncertainty (in %) mentioned in the subsequent results encompasses all the uncertainties associated with the components used to calculate  $C_X$  (e.g., ion signals, MFC,  $P_{\text{vap}}$ ,  $\Delta H_{\text{vap/sub}}$ ) (Sect. S1 in the Supplement).

### 2.2.4 Experimental calibration with sulfuric acid

To make accurate comparisons between our laboratory studies, field results, and reports in the literature, we also calibrated the  $\text{NO}_3^-$  ToFCIMS instrument using  $\text{H}_2\text{SO}_4$  as calibrant, which is a procedure employed in several studies (e.g., Rissanen et al., 2014; Mutzel et al., 2015; Pullinen et al., 2020). This calibration procedure includes generating a specific amount of  $\text{OH}\cdot$  in the presence of excess  $\text{SO}_2$  that reacts to form  $\text{H}_2\text{SO}_4$ , following Reactions (R1), (R2), (R3), and (R4). A calibration unit, developed based on the work of Kürten et al. (2012), was used. It consists of a mercury lamp providing 184.9 nm UV radiation and a quartz glass tube to

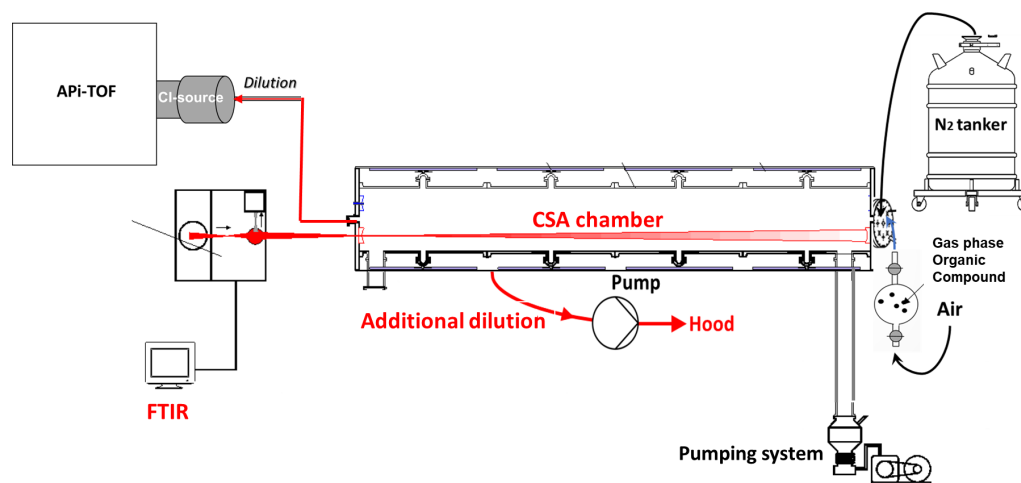
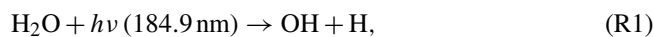


**Figure 3.** The experimental setup to deduce the sensitivity of  $\text{NO}_3^-$  ToFCIMS to an organic compound from its concentration derived by FTIR spectrometry using the CSA chamber.

which a flow of humidified air is added.  $\text{OH}\cdot$  radicals are generated from the photolysis of water vapor by the ultraviolet radiation, which is followed by these reactions:



Three calibration setups were constructed for the  $\text{NO}_3^-$  ToFCIMS instrument (Table 4). In the first setup, the calibration source was connected to the instrument using a Swagelok tee (to overfill the inlet). The second setup involved connecting the calibration unit to the ToFCIMS through a 1 m, 3/4 in. stainless-steel tube (also with a tee to overfill). This line was used to sample ambient air during field campaigns. Finally, the third setup replicated the apparatus employed in the calibration approach described in Sect. 2.2.1 and Fig. 1, which was used to apply calibration approach 1. In this configuration, the sulfuric acid calibration source replaced the ST, and, notably, no heating was applied. The first two setups were designed to assess the wall loss of sulfuric acid in a 1 m sampling tube. The third setup was conducted to collect data to compare the calibration factors obtained from the  $\text{H}_2\text{SO}_4$  source and the organic compounds that were tested.

To conduct a calibration experiment, a range of  $\text{H}_2\text{SO}_4$  concentrations were generated. The  $\text{SO}_2$  concentration was kept constant while varying the  $\text{H}_2\text{O}$  concentrations, which results in different  $\text{OH}$  concentrations.  $\text{SO}_2$  was delivered from an ALPHAGAZ<sup>TM</sup> Mix cylinder (9.04 ppm in a mix of  $\text{N}_2$  and  $\text{O}_2$ ) to create a mixing ratio of about 770 ppbv in the source. To prevent absorption of UV light by ambient  $\text{O}_2$  and  $\text{H}_2\text{O}$  vapor in the space between the mercury

lamp and the quartz tube, the unit was purged with dry  $\text{N}_2$  (ALPHAGAZ 2). The  $\text{H}_2\text{O}$  vapor mixture was generated by passing an airstream through an ultrapure-water bubbler.

The  $\text{H}_2\text{O}$  vapor mixing ratio and  $\text{OH}$  concentration are determined using Eqs. (6) and (7), respectively.

$$[\text{H}_2\text{O}] = \frac{Q_{\text{H}_2\text{O}}}{Q_{\text{H}_2\text{O}} + Q_{\text{SO}_2} + Q_{\text{air}} + Q_{\text{N}_2}} \times \frac{p_{\text{sat}}(T) \times N_{\text{A}}}{R \times T}, \quad (6)$$

where  $Q_{\text{H}_2\text{O}}$ ,  $Q_{\text{SO}_2}$ ,  $Q_{\text{air}}$ , and  $Q_{\text{N}_2}$  are the flow rates of humidified air,  $\text{SO}_2$  mixture, dry air, and  $\text{N}_2$ , respectively;  $p_{\text{sat}}(T)$  is the saturation vapor pressure of water, at temperature  $T$ , calculated using the Antoine equation (Bridgeman and Aldrich, 1964);  $N_{\text{A}}$  is Avogadro's number; and  $R$  is the ideal gas constant.

$$[\text{OH}] = I \times t_{\text{r}} \times \sigma_{\text{H}_2\text{O}} \times \Phi_{\text{H}_2\text{O}} \times [\text{H}_2\text{O}], \quad (7)$$

where  $I$  is the photon flux ( $\text{photons cm}^{-2} \text{ s}^{-1}$ ) and  $t_{\text{r}}$  is the illumination time (s). The quantity  $I \times t_{\text{r}}$  is determined from actinometry experiments based on the photolysis of  $\text{N}_2\text{O}$  producing  $\text{NO}_x$  (Kürten et al., 2012),  $\sigma_{\text{H}_2\text{O}}$  is the absorption cross section of water vapor at 184.9 nm (Cantrell et al., 1997),  $\Phi_{\text{H}_2\text{O}}$  is the photolysis quantum yield assumed equal to 1, and  $[\text{H}_2\text{O}]$  is the concentration of water calculated from Eq. (6).

The various parameters and the values used in this study are listed in Table 5.

The concentrations of  $\text{H}_2\text{SO}_4$  were estimated by assuming that all  $\text{OH}$  radicals produced react with  $\text{SO}_2$ . The  $\text{H}_2\text{SO}_4$  calibration factors, denoted as  $C(\text{sulfuric})$ , were calculated using Eq. (1).

**Table 4.** Experimental setups for the  $\text{H}_2\text{SO}_4$  calibration source. slpm stands for standard liters per minute.

Setup no.	Inlet sampling flow (slpm)	Comments
1	8	connected to the inlet using a Swagelok tee
2	8	connected to a 1 m length tube (ACROSS campaign setup)
3	6	connected to apparatus used in calibration approach 1 (heated ST)

**Table 5.** Parameters employed in the  $\text{H}_2\text{SO}_4$  source used during calibration experiments of the  $\text{NO}_3^-$  ToFCIMS.

Parameter	Value	Units
$Q_{\text{H}_2\text{O}}$	10–300	sccm
$Q_{\text{N}_2}$	0.098	slpm
$Q_{\text{SO}_2}$	1.08	slpm
$Q_{\text{air}}$	11.4	slpm
$p_{\text{sat}}(T)$	0.02771	atm
$N_{\text{A}}$	$6.022 \times 10^{23}$	molec. $\text{cm}^{-3} \text{mol}^{-1}$
$T$	23	$^{\circ}\text{C}$
$R$	0.08206	$\text{L atm mol}^{-1} \text{K}^{-1}$
$I \times t_{\text{r}}$	$2.1 \times 10^{11}$	photons $\text{cm}^{-2}$
$\sigma_{\text{H}_2\text{O}}$	$7.22 \times 10^{-20}$	$\text{cm}^2 \text{molec.}^{-1}$
$\Phi_{\text{H}_2\text{O}}$	1	–

### 3 Results

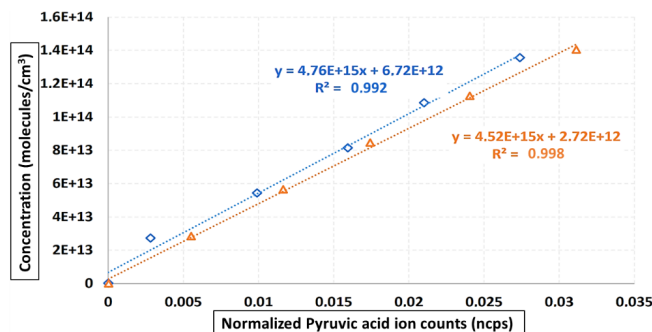
#### 3.1 Outcomes from approach 1 (heated ST)

##### 3.1.1 Pyruvic acid (PyA)

Two experiments were conducted by putting a piece of glass wool with small amount of pyruvic acid (monocarboxylic acid,  $\text{C}_3\text{H}_4\text{O}_3$ ) in the ST. The  $P_{\text{vap}}(\text{PyA})$  at a specific  $T$  was calculated using Eq. (3) with a literature value for the standard molar enthalpy of vaporization  $\Delta H_{\text{vap}}(\text{PyA})$  at 298.15 K of  $53.6 \pm 2.1 \text{ kJ mol}^{-1}$  (Emel'yanenko et al., 2018). The calculation used a  $P_{\text{vap}}$  of  $289.9 \pm 7.3 \text{ Pa}$  at a temperature of 308.2 K (Emel'yanenko et al., 2018). The normalized ToFCIMS signals of  $\text{C}_3\text{H}_4\text{O}_3$  showed a linear increase with the flow through to the ST ( $R^2 = 0.98$ ; see Fig. 4). The  $C(\text{PyA})$  values from both experiments yielded an average of  $4.64 \times 10^{15} \text{ molec. cm}^{-3}$  with 5 % of total uncertainty. By comparing this result with the values reported in the literature (Table 2), one can conclude that  $\text{NO}_3^-$  ToFCIMS exhibits low sensitivity to  $\text{C}_3\text{H}_4\text{O}_3$  despite its high O/C ratio. The ratio between ions of the deprotonated form ( $\text{C}_3\text{H}_3\text{O}_3^-$ ;  $m/z$  87.0087) and the ion of the cluster forms ( $\text{C}_3\text{H}_4\text{O}_3 \cdot \text{NO}_3^-$ ;  $m/z$  150.0044) is about 0.56.

##### 3.1.2 Oxalic acid (OxA)

Several experiments were performed to evaluate the sensitivity of the instrument towards oxalic acid ( $\text{C}_2\text{H}_2\text{O}_4$ ) using

**Figure 4.**  $\text{NO}_3^-$  ToFCIMS sensitivity to pyruvic acid derived from the linear fit to the injected concentration versus the pyruvic acid ion signals normalized to the total ion count of the reagent ions (ion ratio) for the two conducted experiments.

approach 1 (heated ST). An average of the solid  $P_{\text{vap}}(\text{OxA})$  (298 K) values reported in the literature was used in Eq. (3) ( $P_{\text{vap,avg}} = 1.89 \pm 0.8 \times 10^{-2} \text{ Pa}$ ) (Noyes and Wobbe, 1926; Bradley and Cotson, 1953; de Wit et al., 1983; Booth et al., 2010). The  $P_{\text{vap}}$  at the experimental  $T$  was calculated according to Eq. (3) by taking the average of the published sublimation enthalpies  $\Delta H_{\text{sub}}(\text{OxA}) = 91 \pm 9 \text{ kJ mol}^{-1}$  (average taken from Bilde et al., 2015). Figure 5 shows the  $C(\text{OxA})$  obtained. The average value obtained for  $C(\text{OxA})$  was  $1.16 \times 10^{13} \text{ molec. cm}^{-3}$  with 44 % of total uncertainty. This value is about 3 orders of magnitude greater than the calibrations values reported in the literature for HOMs (meaning less sensitive). Yet, it is more than 2 orders of magnitude less than the value reported for malonic acid (Table 2). Once again, despite its high O/C ratio, the results suggest that the  $\text{NO}_3^-$  ToFCIMS exhibits lower sensitivity towards  $\text{C}_2\text{H}_2\text{O}_4$  but demonstrates better sensitivity than  $\text{C}_3\text{H}_4\text{O}_3$ . The ratio between ions of the deprotonated form ( $\text{C}_2\text{HO}_4^-$ ;  $m/z$  88.9880) and the ion of the cluster forms ( $\text{C}_2\text{H}_2\text{O}_4 \cdot \text{NO}_3^-$ ;  $m/z$  151.9836) is about 0.14.

##### 3.1.3 Succinic acid (SucA)

Several experiments were conducted to evaluate the response of the instrument to succinic acid ( $\text{C}_4\text{H}_6\text{O}_4$ ). The solid  $P_{\text{vap}}(\text{SucA})$  (298 K) is equal to  $(7.7 \pm 5.0) \times 10^{-5} \text{ Pa}$  from the review of Bilde et al. (2015).  $P_{\text{vap}}(T)$  has also been calculated according to Eq. (3) by taking the average of the published sublimation enthalpies

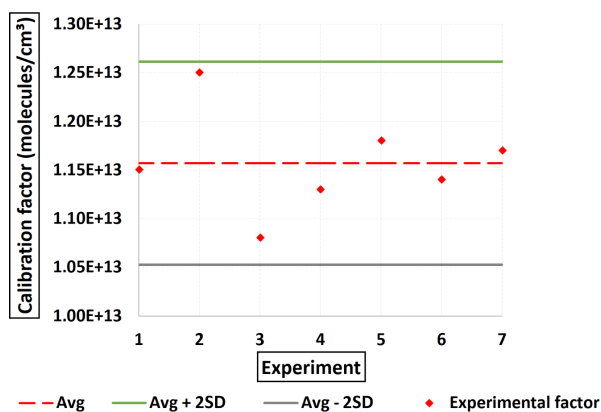


**Figure 5.** Oxalic acid calibration coefficients obtained showing the mean (red line) and 95 % confidence intervals (green and gray lines). The red symbols depict the calibration factors obtained from each experiment.

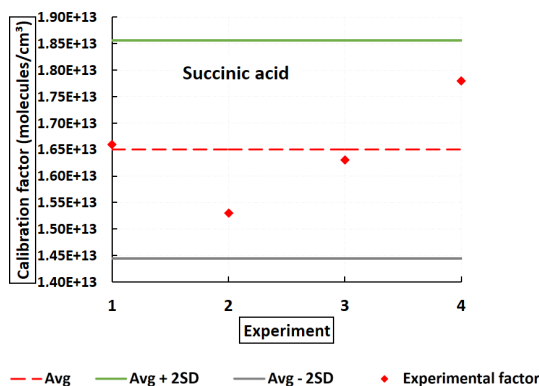


**Figure 6.** Succinic acid calibration coefficients obtained. The red symbols depict the calibration factors obtained from each experiment performed.

$\Delta H_{\text{sub}}(\text{SucA}) = (115 \pm 15) \text{ kJ mol}^{-1}$ . An average value of  $C(\text{SucA}) = 1.65 \times 10^{13} \text{ molec. cm}^{-3}$  was achieved with about 66 % of total uncertainty. Figure 6 shows the  $C(\text{SucA})$  obtained from four successful tests. They are close to the one obtained for  $\text{C}_2\text{H}_2\text{O}_4$ . It is still approximately 3 orders of magnitude greater (meaning less sensitive) than the values reported for  $\text{H}_2\text{SO}_4$  and the organic calibrants in the literature (Table 2). This indicates that the  $\text{NO}_3^-$  ToFCIMS exhibits a rather low sensitivity towards  $\text{C}_4\text{H}_6\text{O}_4$  in comparison to  $\text{H}_2\text{SO}_4$  detection. The ratio between ions of the deprotonated form ( $\text{C}_4\text{H}_5\text{O}_4^-$ ;  $m/z$  117.0193) and the ion of the cluster forms ( $\text{C}_4\text{H}_6\text{O}_4 \cdot \text{NO}_3^-$ ;  $m/z$  180.0149) is about 0.16.

### 3.1.4 Malonic acid (MA)

Following the procedure described in Sect. 2.2.2, an experimental mean value of  $P_{\text{vap}}(\text{MA})$  (323 K)  $= (1.48 \pm 0.15) \times 10^{-2} \text{ Pa}$  was obtained.  $P_{\text{vap}}(\text{MA})$  (298 K)  $= 4.50 \times 10^{-4} \text{ Pa}$  was determined using Eq. (3),

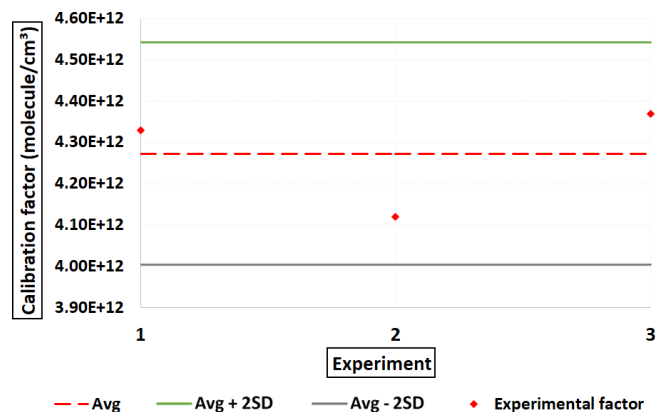


**Figure 7.** Malonic calibration coefficients obtained within a 95 % confidence interval. The red symbols depict the factors obtained from each experiment performed.

employing the average of three published sublimation enthalpies  $\Delta H_{\text{sub}}(\text{MA}) = (111.8 \pm 14) \text{ kJ mol}^{-1}$  (Ribeiro da Silva et al., 1999; Booth et al., 2010; Cappa et al., 2008). This experimental value for the vapor pressure of malonic acid is comparable to the average of  $P_{\text{vap}}(\text{MA})$  (298 K)  $= 4.88 \times 10^{-4} \text{ Pa}$  obtained in these studies, employing Eq. (4) and method described in Sect. 2.2.2, with a relative difference of 7.7 %. Our experimental value was used to estimate the calibration factor for  $\text{C}_3\text{H}_4\text{O}_4$ .

An average value of  $C(\text{MA}) = 4.27 \times 10^{12} \text{ molec. cm}^{-3}$  was achieved with about 30 % of total uncertainty (Fig. 7). This value is about 2 orders of magnitude greater than that the one reported by Krechmer et al. (2015) and Massoli et al. (2018) (Table 2) but lower than the calibration factor values obtained for  $\text{C}_2\text{H}_2\text{O}_4$ ,  $\text{C}_3\text{H}_4\text{O}_3$  and  $\text{C}_4\text{H}_6\text{O}_4$ . This indicates that the  $\text{NO}_3^-$  ToFCIMS exhibits higher sensitivity towards  $\text{C}_3\text{H}_4\text{O}_4$  compared to the other compounds that were tested. Nevertheless, there is a lack of adequate evidence to elucidate these discrepancies. The ratio between ions of the deprotonated form ( $\text{C}_3\text{H}_3\text{O}_4^-$ ;  $m/z$  103.0036) and the ion of the cluster forms ( $\text{C}_3\text{H}_4\text{O}_4 \cdot \text{NO}_3^-$ ;  $m/z$  165.9993) is approximately 0.17.

### 3.1.5 Tartaric acid (TA)

For calibration of the instrument to tartaric acid ( $\text{C}_4\text{H}_6\text{O}_6$ ), the  $P_{\text{vap}}(\text{TA})$  (298 K)  $= (1.79 \pm 0.72) \times 10^{-4} \text{ Pa}$  was taken from Booth et al. (2010), who reported the only experimentally obtained values of  $P_{\text{vap}}(\text{TA})$  and  $\Delta H_{\text{sub}}(\text{TA})$ . Similarly to the other molecules studied,  $P_{\text{vap}}(\text{TA})(T)$  was calculated using Eq. (3) with  $\Delta H_{\text{sub}}(\text{TA}) = (68 \pm 10) \text{ kJ mol}^{-1}$  (Booth et al., 2010). The average value obtained in this study for  $C(\text{TA})$  is  $5.84 \times 10^{12} \text{ molec. cm}^{-3}$ , with an estimated 43 % total uncertainty. Figure 8 shows the  $C(\text{TA})$  values obtained. This value is similar to that obtained for  $\text{C}_3\text{H}_4\text{O}_4$  in this study. However, it is still approximately 2 orders of magnitude higher than the values reported in the literature for

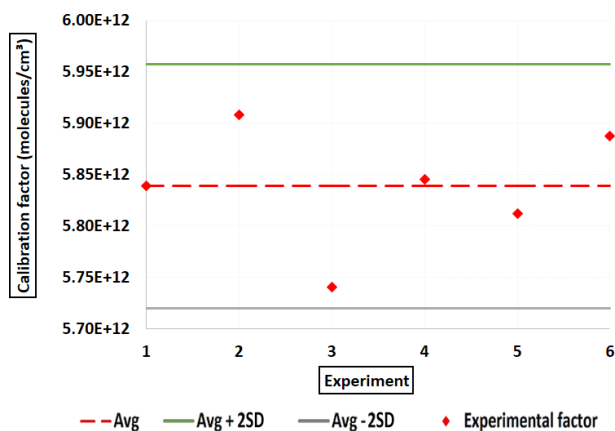


**Figure 8.** Tartaric calibration coefficients obtained within a 95 % confidence interval. The red symbols depict the factors obtained from each experiment performed.

$\text{H}_2\text{SO}_4$ , which is used for HOMs. The ratio between ions of the deprotonated form ( $\text{C}_4\text{H}_5\text{O}_5^-$ ;  $m/z$  149.0091) and the ion of the cluster forms ( $\text{C}_4\text{H}_6\text{O}_6 \cdot \text{NO}_3^-$ ;  $m/z$  212.0048) is approximately 1.

### 3.1.6 4-Nitrocatechol (4-NC)

The  $P_{\text{vap}}(4\text{-NC})$  (313 K) equals  $(1.49 \pm 0.55) \times 10^{-3}$  Pa, which was determined experimentally in the laboratory following the approach used for  $P_{\text{vap}}(4\text{-NC})$  (323 K), described in Sect. 2.2.2. Using  $\Delta H_{\text{sub}}(4\text{-NC}) = (121.1 \pm 1.4) \text{ kJ mol}^{-1}$  (Ribeiro da Silva et al., 1986),  $P_{\text{vap}}(4\text{-NC})$  (298 K) can be determined using Eq. (3). An average value of  $C(4\text{-NC}) = 1.49 \times 10^{11} \text{ molec. cm}^{-3}$  was obtained with an estimated total uncertainty of 16 % (Fig. 9). Among all the tested organic compounds, 4-nitrocatechol demonstrates the lowest  $C_X$ , indicating that, of the compounds studied, the instrument is more sensitive towards this molecule. However, even with this better sensitivity,  $\text{C}_6\text{H}_5\text{NO}_4$  still exhibits values approximately 1 order of magnitude higher than those reported the literature for  $\text{H}_2\text{SO}_4$ . The ratio between ions of the deprotonated form ( $\text{C}_6\text{H}_4\text{NO}_4^-$ ;  $m/z$  154.0145) and the ion of the cluster forms ( $\text{C}_6\text{H}_5\text{NO}_4 \cdot \text{NO}_3^-$ ;  $m/z$  217.0102) is approximately 0.7.

## 3.2 Outcomes from approach 2 (CSA)

Following approach 2, two experiments were carried out by adding pyruvic acid to the CSA chamber. Figure 10 displays the time series of PyA concentrations as determined by FTIR, and the corresponding normalized ion signals from the  $\text{NO}_3^-$  ToFCIMS for the two experiments, labeled as experiment 1 and experiment 2, are shown. The yellow shaded regions in the figure represent the periods during which dilution was introduced into the chamber.

Furthermore, when fitting the pyruvic concentrations measured via FTIR against the normalized PyA ion signals ac-

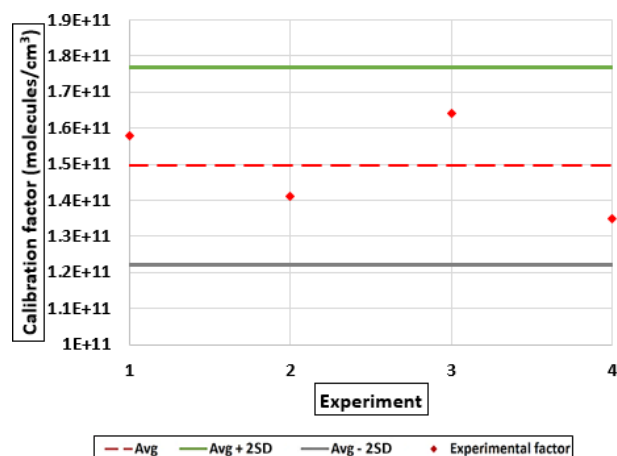


**Figure 9.** 4-Nitrocatechol calibration coefficients obtained within a 95 % confidence interval. The red symbols depict the factors obtained from each experiment performed.

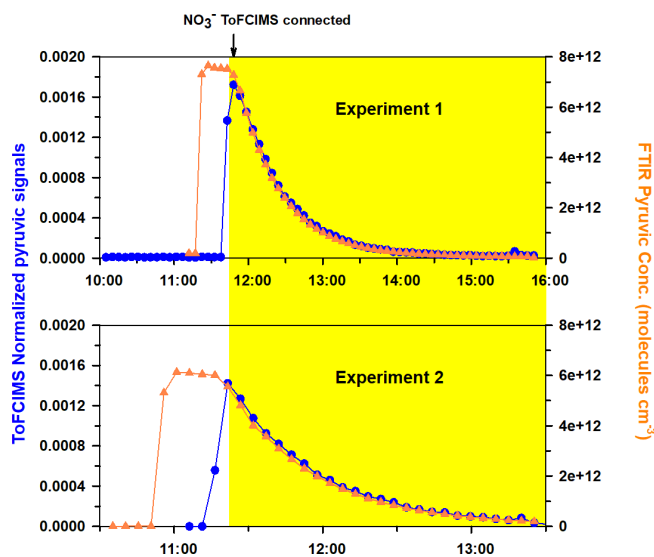


**Figure 10.** Time series of pyruvic acid concentrations obtained by FTIR and the corresponding normalized ion signals from the  $\text{NO}_3^-$  ToFCIMS.

quired from ToFCIMS, the resulting slope corresponds to the pyruvic acid calibration factor, denoted as  $C(\text{PyA})$  (see Fig. 11). Individual values can be calculated using Eq. (8).

$$C(\text{PyA}) = \frac{[\text{PyA}]_{\text{FTIR}} (\text{molec. cm}^{-3})}{\text{ion ratio}_{\text{PyA}}}, \quad (8)$$

where  $C(\text{PyA})$  is the calibration factor in  $\text{molec. cm}^{-3} / \text{ion ratio}$ ,  $[\text{PyA}]_{\text{FTIR}}$  represents the concentrations obtained from the FTIR analysis in  $\text{molec. cm}^{-3}$ , and  $\text{ion ratio}_{\text{PyA}}$  represents the normalized ion signals for pyruvic acid obtained with the ToFCIMS.

The average value of  $C(\text{PyA})$  from these experiments is  $(3.81 \pm 0.03) \times 10^{15} \text{ molec. cm}^{-3} / \text{ion ratio}$ . The relative

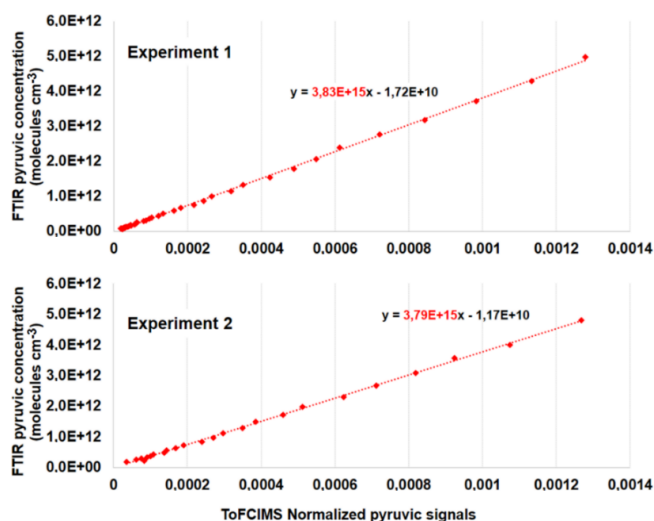


**Figure 11.** FTIR pyruvic acid concentration vs. normalized pyruvic acid signals of ToFCIMS. The dashed red lines are the fitted trend lines. The slopes equal the calibration factor for each experiment.

difference between this value and the one obtained by approach 1 is 18%. This difference could be explained by various factors, including uncertainties in the values of  $P_{\text{vap}}(\text{PyA})$  and  $\Delta H_{\text{sub}}(\text{PyA})$  used in the calculation of approach 1 and the uncertainties in the IR reference spectrum employed in approach 2. However, in both cases, the  $C(\text{PyA})$  value obtained in this study is about 5 orders of magnitude greater than the factors found in the literature using  $\text{H}_2\text{SO}_4$  as calibrant (Table 2), confirming that our  $\text{NO}_3^-$  ToFCIMS exhibits low sensitivity towards  $\text{C}_3\text{H}_4\text{O}_3$ .

Table 6 provides a summary of the calibration factors obtained for the small dicarboxylic acids and 4-nitrocatechol. The findings highlight a significant variability in the calibration factors, illustrating that the sensitivity of the  $\text{NO}_3^-$  ToFCIMS is compound-specific, particularly for these small OVOCs.

### 3.3 Outcomes from calibration with sulfuric acid

Table 7 summarizes the sulfuric acid calibration factors  $C(\text{sulfuric})$  obtained using the different experimental setup. The  $C(\text{sulfuric})$  values obtained from the three setups are within the range reported in the literature ( $0.165\text{--}6) \times 10^{10}$  molec.  $\text{cm}^{-3}$  / ion ratio (see Table 2). Comparing setups 1 and 2 revealed a loss of approximately 33% in  $\text{H}_2\text{SO}_4$  levels along the 1 m sampling line.

Furthermore, we notice that the  $C(\text{sulfuric})$  obtained from setup 3 differs significantly from those obtained for organic acids but reveals a loss of 65% with the setup used. This loss alone cannot explain the differences observed in the literature for the different OVOCs tested and strength the studies done by Hyttinen et al. (2015) and Tröstl et al. (2016), showing the compound-specific sensitivity of this instrument.

**Table 6.** Summary of the calibration factors results for the organic compound acid measured with the  $\text{NO}_3^-$  ToFCIMS.

Compound	$C_x$ (molec. $\text{cm}^{-3}$ )
Pyruvic acid	$4.64 \times 10^{15a}$ $3.81 \times 10^{15b}$
Succinic acid	$1.65 \times 10^{13a}$
Oxalic acid	$1.16 \times 10^{13a}$
Tartaric acid	$5.84 \times 10^{12a}$
Malonic acid	$4.27 \times 10^{12a}$
4-nitrocatechol	$1.49 \times 10^{11a}$

<sup>a</sup> Following approach 1 (heated ST). <sup>b</sup> Following approach 2 (CSA).

**Table 7.** The calibration factor deriving from three experimental setups.

Setup no.	$C(\text{sulfuric})$ (molec. $\text{cm}^{-3}$ )
1	$2.82 \times 10^9$
2	$4.22 \times 10^9$
3	$8.07 \times 10^9$

## 4 Conclusion

Instrument calibration is a crucial step in ensuring the accuracy and reliability of analytical tools. Typically, the  $\text{NO}_3^-$  ToFCIMS instrument is calibrated using sulfuric acid, and the resulting calibration factor  $C(\text{sulfuric})$  is used to quantify all detected species, including HOMs. It should be noted that HOM concentrations should be considered as lower limits. In our efforts to find more suitable and reliable organic calibrants, we implemented calibration procedures for the  $\text{NO}_3^-$  ToFCIMS instrument to assess its sensitivity and linearity in detecting various commercially available organic compounds.

The tested organic compound calibrants for the  $\text{NO}_3^-$  ToFCIMS are summarized in Table 3.

Our studies demonstrate substantial variability in the calibration factors (Table 6) obtained for the small dicarboxylic acids and 4-nitrocatechol. Notably, 4-nitrocatechol exhibited the highest sensitivity, followed by malonic acid, tartaric acid, oxalic acid, and succinic acid, with pyruvic acid being the least sensitive. This shows that the sensitivity of the  $\text{NO}_3^-$  ToFCIMS is dependent on the specific structure of the organic compound. Therefore, relying on a single calibration factor obtained from  $\text{H}_2\text{SO}_4$  does not seem to be appropriate for quantifying all species detected using this technique. The calibration factor for pyruvic acid showed

good agreement between approach 1 and 2 with a relative difference of 18 %. We observed that the calibration factor for malonic acid is approximately 2 orders of magnitude higher than values reported in the literature without any apparent explanation. When considering all the  $C_X$  values in Table 2, an average value of  $2.02 \times 10^{10}$  molec.  $\text{cm}^{-3}$  is obtained ( $\sigma = 1.96 \times 10^{10}$  molec.  $\text{cm}^{-3}$ ). This average is roughly 1 order of magnitude less than the one obtained for 4-nitrocatechol by our instrument, more than 2 orders of magnitude less than malonic and tartaric acid, 3 orders of magnitude lower than oxalic and succinic acid, and more than 5 orders of magnitude less than pyruvic acid. The tested compounds are probably not suitable to account for HOM calibration factors because of their oxidation state or chemical structure, which differs from that of HOMs. Furthermore, the relative contribution of various ionization reaction pathways cannot explain the differences observed for  $C_X$  between the various OVOCs tested.

Additionally, the conventional calibration method for the  $\text{NO}_3^-$  ToFCIMS using  $\text{H}_2\text{SO}_4$  was applied following an approach similar to that in Kürten et al. (2012). This calibration was implemented using three different setups in the laboratory (Table 4), with the calibration factors obtained ( $2.83\text{--}8.08 \times 10^9$  molec.  $\text{cm}^{-3}$ ) being within the reported range in the literature ( $0.2\text{--}6 \times 10^{10}$  molec.  $\text{cm}^{-3}$ ), excluding an instrumental malfunctioning as a plausible explanation for disagreement observed between  $C_X$  for OVOCs determined in this study and  $C_X$  from the literature. A comparison between setups 1 and 2 indicated a loss of approximately 33 % in  $\text{H}_2\text{SO}_4$  levels along the 1 m sampling line. Therefore, differences in the loss at the surfaces for HOMs may also lead to differences in the calibration factors. Comparatively, the  $C(\text{sulfuric})$  values derived from setup 3 differ substantially from those obtained for organic acids using our calibration approaches 1 and 2.

In summary, the calibration experiments have underscored the limitations of using sulfuric acid for establishing calibration factors for quantificational detected compounds, especially small dicarboxylic acids. Without an existing alternative, sulfuric acid is used to quantify all the species detected by the  $\text{NO}_3^-$  ToFCIMS, including HOMs. To ensure the relevance of such approach, it is crucial to identify and investigate organic compounds that more accurately represent the properties of HOMs, providing a more reliable and precise means of quantifying HOMs. The calibration factors obtained using these new compounds should be compared with those obtained using sulfuric acid. Given that such compounds may not be readily available commercially, their synthesis in the laboratory becomes a necessity, although a difficult step needs to be undertaken.

It should be recognized, however, that each instrument has a unique set of operational parameters that dictate its performance, sensitivity, and detection capabilities. Factors such as the design and length of the sampling line, its diameter, and the sampling environment (e.g., temperature and humidity)

can significantly impact the accuracy and representativeness of the analyzed sample. These factors may vary depending on the instrument's location, further highlighting the need for careful consideration.

*Data availability.* ToFCIMS data and calibrations from ACROSS campaign can be found at <https://doi.org/10.25326/576> (Cantrell et al., 2023). Laboratory experiment data for calibration and sensitivity assessment are available upon request.

*Supplement.* The supplement related to this article is available online at: <https://doi.org/10.5194/amt-17-4709-2024-supplement>.

*Author contributions.* SH, VM, and CC came up with the research idea, with VM and CC providing oversight throughout the work's development. SH, VM, SH, BPV, MC, and CC actively participated in the CSA chamber experiments. MR and AK facilitated the experiments by providing the sulfuric acid calibration unit. SH conducted laboratory experiments, analyzed the results, and drafted the initial manuscript. CC and VM reviewed and refined the manuscript for clarity and coherence. All co-authors contributed substantially to the discussions and provided valuable feedback on the manuscript.

*Competing interests.* The contact author has declared that none of the authors has any competing interests.

*Disclaimer.* Publisher's note: Copernicus Publications remains neutral with regard to jurisdictional claims made in the text, published maps, institutional affiliations, or any other geographical representation in this paper. While Copernicus Publications makes every effort to include appropriate place names, the final responsibility lies with the authors.

*Special issue statement.* This article is part of the special issue "Atmospheric Chemistry of the Suburban Forest – multiplatform observational campaign of the chemistry and physics of mixed urban and biogenic emissions". It is not associated with a conference.

*Acknowledgements.* This work has been supported by the ACROSS project. Data from the ACROSS campaign are hosted by the French national center for atmospheric data and services AERIS. This work has also been supported by the region of Paris in the framework of a call for projects from DIM QI<sup>2</sup>.

The authors also want to thank the ICARE institute and especially Wahid Mellouki and Véronique Daële for lending their ToFCIMS inlet, without which this study would not have been possible. Helpful comments by the reviewers are gratefully acknowledged.

*Financial support.* The ACROSS project has been supported by the French National Research Agency (Agence Nationale de la Recherche, ANR) under the investment program integrated into France 2030 (ANR-17-MPGA-0002); the French national program LEFE (Les Enveloppes Fluides et l'Environnement) of the Centre National de la Recherche Scientifique, Institut National des Sciences de L'Univers (ACROSS-GO); and the region of Paris (DIM QI<sup>2</sup>: INFAMY-TC).

*Review statement.* This paper was edited by Hendrik Fuchs and reviewed by two anonymous referees.

## References

- Berndt, T., Jokinen, T., Sipilä, M., Mauldin, R. L., Herrmann, H., Stratmann, F., Junninen, H., and Kulmala, M.: H<sub>2</sub>SO<sub>4</sub> formation from the gas-phase reaction of stabilized Criegee Intermediates with SO<sub>2</sub>: Influence of water vapour content and temperature, *Atmos. Environ.*, 89, 603–612, <https://doi.org/10.1016/j.atmosenv.2014.02.062>, 2014.
- Berndt, T., Richters, S., Kaethner, R., Voigtländer, J., Stratmann, F., Sipilä, M., Kulmala, M., and Herrmann, H.: Gas-Phase Ozonolysis of Cycloalkenes: Formation of Highly Oxidized RO<sub>2</sub> Radicals and Their Reactions with NO, NO<sub>2</sub>, SO<sub>2</sub>, and Other RO<sub>2</sub> Radicals, *J. Phys. Chem. A*, 119, 10336–10348, <https://doi.org/10.1021/acs.jpca.5b07295>, 2015.
- Berndt, T., Herrmann, H., Sipilä, M., and Kulmala, M.: Highly Oxidized Second-Generation Products from the Gas-Phase Reaction of OH Radicals with Isoprene, *J. Phys. Chem. A*, 120, 10150–10159, <https://doi.org/10.1021/acs.jpca.6b10987>, 2016.
- Berndt, T., Møller, K. H., Herrmann, H., and Kjaergaard, H. G.: Trimethylamine Outruns Terpenes and Aromatics in Atmospheric Autoxidation, *J. Phys. Chem. A*, 125, 4454–4466, <https://doi.org/10.1021/acs.jpca.1c02465>, 2021.
- Bianchi, F., Kurtén, T., Riva, M., Mohr, C., Rissanen, M. P., Roldin, P., Berndt, T., Crouse, J. D., Wennberg, P. O., Mentel, T. F., Wildt, J., Junninen, H., Jokinen, T., Kulmala, M., Worsnop, D. R., Thornton, J. A., Donahue, N., Kjaergaard, H. G., and Ehn, M.: Highly Oxygenated Organic Molecules (HOM) from Gas-Phase Autoxidation Involving Peroxy Radicals: A Key Contributor to Atmospheric Aerosol, *Chem. Rev.*, 119, 3472–3509, <https://doi.org/10.1021/acs.chemrev.8b00395>, 2019.
- Bilde, M., Barsanti, K., Booth, M., Cappa, C. D., Donahue, N. M., Emanuelsson, E. U., McFiggans, G., Krieger, U. K., Marcolli, C., Topping, D., Ziemann, P., Barley, M., Clegg, S., Dennis-Smith, B., Hallquist, M., Hallquist, Å. M., Khlystov, A., Kulmala, M., Mogensen, D., Percival, C. J., Pope, F., Reid, J. P., Ribeiro da Silva, M. A. V., Rosenoern, T., Salo, K., Soonsin, V. P., Yli-Juuti, T., Prisle, N. L., Pagels, J., Rarey, J., Zardini, A. A., and Ripinen, I.: Saturation Vapor Pressures and Transition Enthalpies of Low-Volatility Organic Molecules of Atmospheric Relevance: From Dicarboxylic Acids to Complex Mixtures, *Chem. Rev.*, 115, 4115–4156, <https://doi.org/10.1021/cr5005502>, 2015.
- Booth, A. M., Barley, M. H., Topping, D. O., McFiggans, G., Garforth, A., and Percival, C. J.: Solid state and sub-cooled liquid vapour pressures of substituted dicarboxylic acids using Knudsen Effusion Mass Spectrometry (KEMS) and Differential Scanning Calorimetry, *Atmos. Chem. Phys.*, 10, 4879–4892, <https://doi.org/10.5194/acp-10-4879-2010>, 2010.
- Bradley, R. S. and Cotson, S.: 347. The vapour pressure and lattice energy of hydrogen-bonded crystals. Part II.  $\alpha$ - and  $\beta$ -Anhydrous oxalic acid and tetragonal pentaerythritol, *J. Chem. Soc.*, 1684–1688, <https://doi.org/10.1039/JR9530001684>, 1953.
- Bridgeman, O. C. and Aldrich, E. W.: Vapor Pressure Tables for Water, *J. Heat Transf.*, 86, 279–286, <https://doi.org/10.1115/1.3687121>, 1964.
- Cantrell, C. A., Shetter, R. E., Calvert, J. G., Eisele, F. L., and Tanner, D. J.: Some considerations of the origin of nighttime peroxy radicals observed in MLOPEX 2, *J. Geophys. Res.-Atmos.*, 102, 15899–15913, <https://doi.org/10.1029/97JD01120>, 1997.
- Cappa, C. D., Lovejoy, E. R., and Ravishankara, A. R.: Evidence for liquid-like and nonideal behavior of a mixture of organic aerosol components, *P. Natl. Acad. Sci. USA*, 105, 18687–18691, <https://doi.org/10.1073/pnas.0802144105>, 2008.
- Cantrell, C., Michoud, V., and Alage, S.: ACROSS\_LISA\_RambForest\_ToFCIMS-count\_L2, Aeris [data set], <https://doi.org/10.25326/576>, 2023.
- Cheng, X., Chen, Q., Li, Y., Huang, G., Liu, Y., Lu, S., Zheng, Y., Qiu, W., Lu, K., Qiu, X., Bianchi, F., Yan, C., Yuan, B., Shao, M., Wang, Z., Zhu, T., Wu, Y., and Zeng, L.: Secondary Production of Gaseous Nitrated Phenols in Polluted Urban Environments, *Environ. Sci. Technol.*, 55, 4410–4419, <https://doi.org/10.1021/acs.est.0c07988>, 2021.
- Crouse, J. D., Nielsen, L. B., Jørgensen, S., Kjaergaard, H. G., and Wennberg, P. O.: Autoxidation of Organic Compounds in the Atmosphere, *J. Phys. Chem. Lett.*, 4, 3513–3520, <https://doi.org/10.1021/jz4019207>, 2013.
- Dam, M., Draper, D. C., Marsavin, A., Fry, J. L., and Smith, J. N.: Observations of gas-phase products from the nitrate-radical-initiated oxidation of four monoterpenes, *Atmos. Chem. Phys.*, 22, 9017–9031, <https://doi.org/10.5194/acp-22-9017-2022>, 2022.
- de Wit, H. G. M., Bouwstra, J. A., Blok, J. G., and de Kruif, C. G.: Vapor pressures and lattice energies of oxalic acid, mesotartaric acid, phloroglucinol, myoinositol, and their hydrates, *J. Chem. Phys.*, 78, 1470–1475, <https://doi.org/10.1063/1.444836>, 1983.
- Donahue, N. M., Epstein, S. A., Pandis, S. N., and Robinson, A. L.: A two-dimensional volatility basis set: 1. organic-aerosol mixing thermodynamics, *Atmos. Chem. Phys.*, 11, 3303–3318, <https://doi.org/10.5194/acp-11-3303-2011>, 2011.
- Doussin, J.-F., Durand-Jolibois, R., Ritz, D., Monod, A., and Carlier, P.: Design of an environmental chamber for the study of atmospheric chemistry: New developments in the analytical device, *Analisis*, 25, 236–242, 1997.
- Ehn, M., Kleist, E., Junninen, H., Petäjä, T., Lönn, G., Schobesberger, S., Dal Maso, M., Trimborn, A., Kulmala, M., Worsnop, D. R., Wahner, A., Wildt, J., and Mentel, Th. F.: Gas phase formation of extremely oxidized pinene reaction products in chamber and ambient air, *Atmos. Chem. Phys.*, 12, 5113–5127, <https://doi.org/10.5194/acp-12-5113-2012>, 2012.
- Ehn, M., Thornton, J. A., Kleist, E., Sipilä, M., Junninen, H., Pullinen, I., Springer, M., Rubach, F., Tillmann, R., Lee, B., Lopez-Hilfiker, F., Andres, S., Acir, I.-H., Rissanen, M., Jokinen, T., Schobesberger, S., Kangasluoma, J., Kontkanen, J., Nieminen, T., Kurtén, T., Nielsen, L. B., Jørgensen, S., Kjaergaard, H. G., Canagaratna, M., Maso, M. D., Berndt, T.,

- Petäjä, T., Wahner, A., Kerminen, V.-M., Kulmala, M., Worsnop, D. R., Wildt, J., and Mentel, T. F.: A large source of low-volatility secondary organic aerosol, *Nature*, 506, 476–479, <https://doi.org/10.1038/nature13032>, 2014.
- Ehn, M., Berndt, T., Wildt, J., and Mentel, T.: Highly Oxygenated Molecules from Atmospheric Autoxidation of Hydrocarbons: A Prominent Challenge for Chemical Kinetics Studies, *Int. J. Chem. Kinet.*, 49, 821–831, <https://doi.org/10.1002/kin.21130>, 2017.
- Eisele, F. and Tanner, D.: Measurement of the gas phase concentration of H<sub>2</sub>SO<sub>4</sub> and methane sulfonic acid and estimates of H<sub>2</sub>SO<sub>4</sub> production and loss in the atmosphere, *J. Geophys. Res.*, 98, 9001–9010, 1993.
- Emel'yanenko, V. N., Turovtsev, V. V., and Fedina, Y. A.: Thermodynamic properties of pyruvic acid and its methyl ester, *Thermochim. Acta*, 665, 70–75, <https://doi.org/10.1016/j.tca.2018.05.009>, 2018.
- Field, F. H.: Chemical ionization mass spectrometry, *Accounts Chem. Res.*, 1, 42–49, <https://doi.org/10.1021/ar50002a002>, 1968.
- Finlayson-Pitts, B. J.: Atmospheric chemistry, *P. Natl. Acad. Sci. USA.*, 107, 6566–6567, <https://doi.org/10.1073/pnas.1003038107>, 2010
- Garmash, O., Rissanen, M. P., Pullinen, I., Schmitt, S., Kausiala, O., Tillmann, R., Zhao, D., Percival, C., Bannan, T. J., Priestley, M., Hallquist, Å. M., Kleist, E., Kiendler-Scharr, A., Hallquist, M., Berndt, T., McFiggans, G., Wildt, J., Mentel, T. F., and Ehn, M.: Multi-generation OH oxidation as a source for highly oxygenated organic molecules from aromatics, *Atmos. Chem. Phys.*, 20, 515–537, <https://doi.org/10.5194/acp-20-515-2020>, 2020.
- Guo, Y., Shen, H., Pullinen, I., Luo, H., Kang, S., Vereecken, L., Fuchs, H., Hallquist, M., Acir, I.-H., Tillmann, R., Rohrer, F., Wildt, J., Kiendler-Scharr, A., Wahner, A., Zhao, D., and Mentel, T. F.: Identification of highly oxygenated organic molecules and their role in aerosol formation in the reaction of limonene with nitrate radical, *Atmos. Chem. Phys.*, 22, 11323–11346, <https://doi.org/10.5194/acp-22-11323-2022>, 2022a.
- Guo, Y., Yan, C., Liu, Y., Qiao, X., Zheng, F., Zhang, Y., Zhou, Y., Li, C., Fan, X., Lin, Z., Feng, Z., Zhang, Y., Zheng, P., Tian, L., Nie, W., Wang, Z., Huang, D., Daellenbach, K. R., Yao, L., Dada, L., Bianchi, F., Jiang, J., Liu, Y., Kerminen, V.-M., and Kulmala, M.: Seasonal variation in oxygenated organic molecules in urban Beijing and their contribution to secondary organic aerosol, *Atmos. Chem. Phys.*, 22, 10077–10097, <https://doi.org/10.5194/acp-22-10077-2022>, 2022b.
- Hansel, A., Scholz, W., Mentler, B., Fischer, L., and Berndt, T.: Detection of RO<sub>2</sub> radicals and other products from cyclohexene ozonolysis with NH<sub>4</sub><sup>+</sup> and acetate chemical ionization mass spectrometry, *Atmos. Environ.*, 186, 248–255, <https://doi.org/10.1016/j.atmosenv.2018.04.023>, 2018.
- Hyttinen, N., Kupiainen-Määttä, O., Rissanen, M. P., Muuronen, M., Ehn, M., and Kurtén, T.: Modeling the Charging of Highly Oxidized Cyclohexene Ozonolysis Products Using Nitrate-Based Chemical Ionization, *J. Phys. Chem. A*, 119, 6339–6345, <https://doi.org/10.1021/acs.jpca.5b01818>, 2015.
- Isaacman-VanWertz, G., Massoli, P., O'Brien, R., Lim, C., Franklin, J. P., Moss, J. A., Hunter, J. F., Nowak, J. B., Canagaratna, M. R., Misztal, P. K., Arata, C., Roscioli, J. R., Herndon, S. T., Onasch, T. B., Lambe, A. T., Jayne, J. T., Su, L., Knopf, D. A., Goldstein, A. H., Worsnop, D. R., and Kroll, J. H.: Chemical evolution of atmospheric organic carbon over multiple generations of oxidation, *Nat. Chem.*, 10, 462–468, <https://doi.org/10.1038/s41557-018-0002-2>, 2018.
- Iyer, S., He, X., Hyttinen, N., Kurtén, T., and Rissanen, M. P.: Computational and Experimental Investigation of the Detection of HO<sub>2</sub> Radical and the Products of Its Reaction with Cyclohexene Ozonolysis Derived RO<sub>2</sub> Radicals by an Iodide-Based Chemical Ionization Mass Spectrometer, *J. Phys. Chem. A*, 121, 6778–6789, <https://doi.org/10.1021/acs.jpca.7b01588>, 2017.
- Jokinen, T., Sipilä, M., Junninen, H., Ehn, M., Lönn, G., Hakala, J., Petäjä, T., Mauldin III, R. L., Kulmala, M., and Worsnop, D. R.: Atmospheric sulphuric acid and neutral cluster measurements using CI-API-TOF, *Atmos. Chem. Phys.*, 12, 4117–4125, <https://doi.org/10.5194/acp-12-4117-2012>, 2012.
- Jokinen, T., Sipilä, M., Richters, S., Kerminen, V.-M., Paasonen, P., Stratmann, F., Worsnop, D., Kulmala, M., Ehn, M., Herrmann, H., and Berndt, T.: Rapid Autoxidation Forms Highly Oxidized RO<sub>2</sub> Radicals in the Atmosphere, *Angew. Chem. Int. Ed.*, 53, 14596–14600, <https://doi.org/10.1002/anie.201408566>, 2014.
- Jokinen, T., Berndt, T., Makkonen, R., Kerminen, V.-M., Junninen, H., Paasonen, P., Stratmann, F., Herrmann, H., Guenther, A. B., Worsnop, D. R., Kulmala, M., Ehn, M., and Sipilä, M.: Production of extremely low volatile organic compounds from biogenic emissions: Measured yields and atmospheric implications, *P. Natl. Acad. Sci. USA*, 112, 7123–7128, <https://doi.org/10.1073/pnas.1423977112>, 2015.
- Junninen, H., Ehn, M., Petäjä, T., Luosujärvi, L., Kotiaho, T., Koskiainen, R., Rohner, U., Gonin, M., Fuhrer, K., Kulmala, M., and Worsnop, D. R.: A high-resolution mass spectrometer to measure atmospheric ion composition, *Atmos. Meas. Tech.*, 3, 1039–1053, <https://doi.org/10.5194/amt-3-1039-2010>, 2010.
- Kanakidou, M., Seinfeld, J. H., Pandis, S. N., Barnes, I., Dentener, F. J., Facchini, M. C., Van Dingenen, R., Ervens, B., Nenes, A., Nielsen, C. J., Swietlicki, E., Putaud, J. P., Balkanski, Y., Fuzzi, S., Horth, J., Moortgat, G. K., Winterhalter, R., Myhre, C. E. L., Tsigaridis, K., Vignati, E., Stephanou, E. G., and Wilson, J.: Organic aerosol and global climate modelling: a review, *Atmos. Chem. Phys.*, 5, 1053–1123, <https://doi.org/10.5194/acp-5-1053-2005>, 2005.
- Kirkby, J., Duplissy, J., Sengupta, K., Frege, C., Gordon, H., Williamson, C., Heinritzi, M., Simon, M., Yan, C., Almeida, J., Tröstl, J., Nieminen, T., Ortega, I. K., Wagner, R., Adamov, A., Amorim, A., Bernhammer, A.-K., Bianchi, F., Breitenlechner, M., Brilke, S., Chen, X., Craven, J., Dias, A., Ehrhart, S., Flagan, R. C., Franchin, A., Fuchs, C., Guida, R., Hakala, J., Hoyle, C. R., Jokinen, T., Junninen, H., Kangasluoma, J., Kim, J., Krapf, M., Kürten, A., Laaksonen, A., Lehtipalo, K., Makhmutov, V., Mathot, S., Molteni, U., Onnela, A., Peräkylä, O., Piel, F., Petäjä, T., Praplan, A. P., Pringle, K., Rap, A., Richards, N. A. D., Riipinen, I., Rissanen, M. P., Rondo, L., Sarnela, N., Schobesberger, S., Scott, C. E., Seinfeld, J. H., Sipilä, M., Steiner, G., Stozhkov, Y., Stratmann, F., Tomé, A., Virtanen, A., Vogel, A. L., Wagner, A. C., Wagner, P. E., Weingartner, E., Wimmer, D., Winkler, P. M., Ye, P., Zhang, X., Hansel, A., Dommen, J., Donahue, N. M., Worsnop, D. R., Baltensperger, U., Kulmala, M., Carslaw, K. S., and Curtius, J.: Ion-induced nucleation of pure biogenic particles, *Nature*, 533, 521–526, <https://doi.org/10.1038/nature17953>, 2016.

- Krechmer, J. E., Coggon, M. M., Massoli, P., Nguyen, T. B., Crouse, J. D., Hu, W., Day, D. A., Tyndall, G. S., Henze, D. K., Rivera-Rios, J. C., Nowak, J. B., Kimmel, J. R., Mauldin, R. L., Stark, H., Jayne, J. T., Sipilä, M., Junninen, H., St. Clair, J. M., Zhang, X., Feiner, P. A., Zhang, L., Miller, D. O., Brune, W. H., Keutsch, F. N., Wennberg, P. O., Seinfeld, J. H., Worsnop, D. R., Jimenez, J. L., and Canagaratna, M. R.: Formation of Low Volatility Organic Compounds and Secondary Organic Aerosol from Isoprene Hydroxyhydroperoxide Low-NO Oxidation, *Environ. Sci. Technol.*, 49, 10330–10339, <https://doi.org/10.1021/acs.est.5b02031>, 2015.
- Kürten, A., Rondo, L., Ehrhart, S., and Curtius, J.: Calibration of a Chemical Ionization Mass Spectrometer for the Measurement of Gaseous Sulfuric Acid, *J. Phys. Chem. A*, 116, 6375–6386, <https://doi.org/10.1021/jp212123n>, 2012.
- Kürten, A., Bergen, A., Heinritzi, M., Leiminger, M., Lorenz, V., Piel, F., Simon, M., Sitals, R., Wagner, A. C., and Curtius, J.: Observation of new particle formation and measurement of sulfuric acid, ammonia, amines and highly oxidized organic molecules at a rural site in central Germany, *Atmos. Chem. Phys.*, 16, 12793–12813, <https://doi.org/10.5194/acp-16-12793-2016>, 2016.
- Kurtén, T., Tiusanen, K., Roldin, P., Rissanen, M., Luy, J.-N., Boy, M., Ehn, M., and Donahue, N.:  $\alpha$ -Pinene Autoxidation Products May Not Have Extremely Low Saturation Vapor Pressures Despite High O:C Ratios, *J. Phys. Chem. A*, 120, 2569–2582, <https://doi.org/10.1021/acs.jpca.6b02196>, 2016.
- Luo, H., Vereecken, L., Shen, H., Kang, S., Pullinen, I., Hallquist, M., Fuchs, H., Wahner, A., Kiendler-Scharr, A., Mentel, T. F., and Zhao, D.: Formation of highly oxygenated organic molecules from the oxidation of limonene by OH radical: significant contribution of H-abstraction pathway, *Atmos. Chem. Phys.*, 23, 7297–7319, <https://doi.org/10.5194/acp-23-7297-2023>, 2023.
- Massoli, P., Stark, H., Canagaratna, M. R., Krechmer, J. E., Xu, L., Ng, N. L., Mauldin, R. L., Yan, C., Kimmel, J., Misztal, P. K., Jimenez, J. L., Jayne, J. T., and Worsnop, D. R.: Ambient Measurements of Highly Oxidized Gas-Phase Molecules during the Southern Oxidant and Aerosol Study (SOAS) 2013, *ACS Earth Space Chem.*, 2, 653–672, <https://doi.org/10.1021/acsearthspacechem.8b00028>, 2018.
- Meder, M., Peräkylä, O., Varelas, J. G., Luo, J., Cai, R., Zhang, Y., Kurtén, T., Riva, M., Rissanen, M., Geiger, F. M., Thomson, R. J., and Ehn, M.: Selective deuteration as a tool for resolving autoxidation mechanisms in  $\alpha$ -pinene ozonolysis, *Atmos. Chem. Phys.*, 23, 4373–4390, <https://doi.org/10.5194/acp-23-4373-2023>, 2023.
- Møller, K. H., Bates, K. H., and Kjaergaard, H. G.: The Importance of Peroxy Radical Hydrogen-Shift Reactions in Atmospheric Isoprene Oxidation, *J. Phys. Chem. A*, 123, 920–932, <https://doi.org/10.1021/acs.jpca.8b10432>, 2019.
- Mutzel, A., Poulain, L., Berndt, T., Iinuma, Y., Rodigast, M., Böge, O., Richters, S., Spindler, G., Sipilä, M., Jokinen, T., Kulmala, M., and Herrmann, H.: Highly Oxidized Multifunctional Organic Compounds Observed in Tropospheric Particles: A Field and Laboratory Study, *Environ. Sci. Technol.*, 49, 7754–7761, <https://doi.org/10.1021/acs.est.5b00885>, 2015.
- Noyes Jr., W. A. and Wobbe, D. E.: THE VAPOR PRESSURE OF ANHYDROUS OXALIC ACID, *J. Am. Chem. Soc.*, 48, 1882–1887, <https://doi.org/10.1021/ja01418a012>, 1926.
- Picquet-Varrault, B., Orphal, J., Doussin, J.-F., Carlier, P., and Flaud, J.-M.: Laboratory Intercomparison of the Ozone Absorption Coefficients in the Mid-infrared (10  $\mu$ m) and Ultraviolet (300–350 nm) Spectral Regions, *J. Phys. Chem. A*, 109, 1008–1014, <https://doi.org/10.1021/jp0405411>, 2005.
- Pullinen, I., Schmitt, S., Kang, S., Sarrafzadeh, M., Schlag, P., Andres, S., Kleist, E., Mentel, T. F., Rohrer, F., Springer, M., Tillmann, R., Wildt, J., Wu, C., Zhao, D., Wahner, A., and Kiendler-Scharr, A.: Impact of NO<sub>x</sub> on secondary organic aerosol (SOA) formation from  $\alpha$ -pinene and  $\beta$ -pinene photooxidation: the role of highly oxygenated organic nitrates, *Atmos. Chem. Phys.*, 20, 10125–10147, <https://doi.org/10.5194/acp-20-10125-2020>, 2020.
- Quééléver, L. L. J., Kristensen, K., Normann Jensen, L., Rosati, B., Teiwes, R., Daellenbach, K. R., Peräkylä, O., Roldin, P., Bossi, R., Pedersen, H. B., Glasius, M., Bilde, M., and Ehn, M.: Effect of temperature on the formation of highly oxygenated organic molecules (HOMs) from alpha-pinene ozonolysis, *Atmos. Chem. Phys.*, 19, 7609–7625, <https://doi.org/10.5194/acp-19-7609-2019>, 2019.
- Ribeiro da Silva, M. D. M. C., Ribeiro da Silva, M. A. V., and Pilcher, G.: Enthalpies of combustion of the three trihydroxybenzenes and of 3-methoxycatechol and 4-nitrocatechol, *J. Chem. Thermodyn.*, 18, 295–300, [https://doi.org/10.1016/0021-9614\(86\)90058-3](https://doi.org/10.1016/0021-9614(86)90058-3), 1986.
- Ribeiro da Silva, M. A. V., Monte, M. J. S., and Ribeiro, J. R.: Vapour pressures and the enthalpies and entropies of sublimation of five dicarboxylic acids, *J. Chem. Thermodyn.*, 31, 1093–1107, <https://doi.org/10.1006/jcht.1999.0522>, 1999.
- Riccobono, F., Schobesberger, S., Scott, C. E., Dommen, J., Ortega, I. K., Rondo, L., Almeida, J., Amorim, A., Bianchi, F., Breitenlechner, M., David, A., Downard, A., Dunne, E. M., Duplissy, J., Ehrhart, S., Flagan, R. C., Franchin, A., Hansel, A., Junninen, H., Kajos, M., Keskinen, H., Kupc, A., Kürten, A., Kvashin, A. N., Laaksonen, A., Lehtipalo, K., Makhmutov, V., Mathot, S., Nieminen, T., Onnela, A., Petäjä, T., Praplan, A. P., Santos, F. D., Schallhart, S., Seinfeld, J. H., Sipilä, M., Spracklen, D. V., Stozhkov, Y., Stratmann, F., Tomé, A., Tsagkogeorgas, G., Vaattovaara, P., Viisanen, Y., Virtala, A., Wagner, P. E., Weingartner, E., Wex, H., Wimmer, D., Carslaw, K. S., Curtius, J., Donahue, N. M., Kirkby, J., Kulmala, M., Worsnop, D. R., and Baltensperger, U.: Oxidation products of biogenic emissions contribute to nucleation of atmospheric particles, *Science*, 344, 717–721, <https://doi.org/10.1126/science.1243527>, 2014.
- Riipinen, I., Pierce, J. R., Yli-Juuti, T., Nieminen, T., Häkkinen, S., Ehn, M., Junninen, H., Lehtipalo, K., Petäjä, T., Slowik, J., Chang, R., Shantz, N. C., Abbatt, J., Leaitch, W. R., Kerminen, V.-M., Worsnop, D. R., Pandis, S. N., Donahue, N. M., and Kulmala, M.: Organic condensation: a vital link connecting aerosol formation to cloud condensation nuclei (CCN) concentrations, *Atmos. Chem. Phys.*, 11, 3865–3878, <https://doi.org/10.5194/acp-11-3865-2011>, 2011.
- Rissanen, M.: Anthropogenic Volatile Organic Compound (AVOC) Autoxidation as a Source of Highly Oxygenated Organic Molecules (HOM), *J. Phys. Chem. A*, 125, 9027–9039, <https://doi.org/10.1021/acs.jpca.1c06465>, 2021.
- Rissanen, M., Kurtén, T., Sipilä, M., Thornton, J. A., Kangasluoma, J., Sarnela, N., Junninen, H., Jørgensen, S., Schallhart, S., Kajos, M. K., Taipale, R., Springer, M., Mentel, T. F., Ruuskanen,

- T., Petäjä, T., Worsnop, D. R., Kjaergaard, H. G., and Ehn, M.: The Formation of Highly Oxidized Multifunctional Products in the Ozonolysis of Cyclohexene, *J. Am. Chem. Soc.*, 136, 15596–15606, <https://doi.org/10.1021/ja507146s>, 2014.
- Riva, M., Rantala, P., Krechmer, J. E., Peräkylä, O., Zhang, Y., Heikkinen, L., Garmash, O., Yan, C., Kulmala, M., Worsnop, D., and Ehn, M.: Evaluating the performance of five different chemical ionization techniques for detecting gaseous oxygenated organic species, *Atmos. Meas. Tech.*, 12, 2403–2421, <https://doi.org/10.5194/amt-12-2403-2019>, 2019.
- Schobesberger, S., Junninen, H., Bianchi, F., Lönn, G., Ehn, M., Lehtipalo, K., Dommen, J., Ehrhart, S., Ortega, I. K., Franchin, A., Nieminen, T., Riccobono, F., Hutterli, M., Duplissy, J., Almeida, J., Amorim, A., Breitenlechner, M., Downard, A. J., Dunne, E. M., Flagan, R. C., Kajos, M., Keskinen, H., Kirkby, J., Kupc, A., Kürten, A., Kurtén, T., Laaksonen, A., Mathot, S., Onnela, A., Praplan, A. P., Rondo, L., Santos, F. D., Schallhart, S., Schnitzhofer, R., Sipilä, M., Tomé, A., Tsagkogeorgas, G., Vehkamäki, H., Wimmer, D., Baltensperger, U., Carslaw, K. S., Curtius, J., Hansel, A., Petäjä, T., Kulmala, M., Donahue, N. M., and Worsnop, D. R.: Molecular understanding of atmospheric particle formation from sulfuric acid and large oxidized organic molecules, *P. Natl. Acad. Sci. USA*, 110, 17223–17228, <https://doi.org/10.1073/pnas.1306973110>, 2013.
- Seinfeld, J. H. and Pandis, S. N.: *Atmospheric Chemistry and Physics: From Air Pollution to Climate Change*, 3rd edn., John Wiley & Sons, Inc., Hoboken, New Jersey, ISBN: 9781118947401, 2016.
- Shen, H., Zhao, D., Pullinen, I., Kang, S., Vereecken, L., Fuchs, H., Acir, I.-H., Tillmann, R., Rohrer, F., Wildt, J., Kiendler-Scharr, A., Wahner, A., and Mentel, T. F.: Highly Oxygenated Organic Nitrates Formed from NO<sub>3</sub> Radical-Initiated Oxidation of  $\beta$ -Pinene, *Environ. Sci. Technol.*, 55, 15658–15671, <https://doi.org/10.1021/acs.est.1c03978>, 2021.
- Tröstl, J., Chuang, W. K., Gordon, H., Heinritzi, M., Yan, C., Molteni, U., Ahlm, L., Frege, C., Bianchi, F., Wagner, R., Simon, M., Lehtipalo, K., Williamson, C., Craven, J. S., Duplissy, J., Adamov, A., Almeida, J., Bernhammer, A.-K., Breitenlechner, M., Brilke, S., Dias, A., Ehrhart, S., Flagan, R. C., Franchin, A., Fuchs, C., Guida, R., Gysel, M., Hansel, A., Hoyle, C. R., Jokinen, T., Junninen, H., Kangasluoma, J., Keskinen, H., Kim, J., Krapf, M., Kürten, A., Laaksonen, A., Lawler, M., Leiminger, M., Mathot, S., Möhler, O., Nieminen, T., Onnela, A., Petäjä, T., Piel, F. M., Miettinen, P., Rissanen, M. P., Rondo, L., Sarnela, N., Schobesberger, S., Sengupta, K., Sipilä, M., Smith, J. N., Steiner, G., Tomé, A., Virtanen, A., Wagner, A. C., Weingartner, E., Wimmer, D., Winkler, P. M., Ye, P., Carslaw, K. S., Curtius, J., Dommen, J., Kirkby, J., Kulmala, M., Riipinen, I., Worsnop, D. R., Donahue, N. M., and Baltensperger, U.: The role of low-volatility organic compounds in initial particle growth in the atmosphere, *Nature*, 533, 527–531, <https://doi.org/10.1038/nature18271>, 2016.
- Vereecken, L. and Nozière, B.: H migration in peroxy radicals under atmospheric conditions, *Atmos. Chem. Phys.*, 20, 7429–7458, <https://doi.org/10.5194/acp-20-7429-2020>, 2020.
- Wang, Y., Riva, M., Xie, H., Heikkinen, L., Schallhart, S., Zha, Q., Yan, C., He, X. C., Peräkylä, O., and Ehn, M.: Formation of Highly Oxygenated Organic Molecules from Chlorine-Atom-Initiated Oxidation of Alpha-Pinene, *Atmos Chem Phys*, 20, 5145, 2020.
- Wang, Y., Clusius, P., Yan, C., Dällenbach, K., Yin, R., Wang, M., He, X.-C., Chu, B., Lu, Y., Dada, L., Kangasluoma, J., Rantala, P., Deng, C., Lin, Z., Wang, W., Yao, L., Fan, X., Du, W., Cai, J., Heikkinen, L., Tham, Y. J., Zha, Q., Ling, Z., Junninen, H., Petäjä, T., Ge, M., Wang, Y., He, H., Worsnop, D. R., Kerminen, V.-M., Bianchi, F., Wang, L., Jiang, J., Liu, Y., Boy, M., Ehn, M., Donahue, N. M., and Kulmala, M.: Molecular Composition of Oxygenated Organic Molecules and Their Contributions to Organic Aerosol in Beijing, *Environ. Sci. Technol.*, 56, 770–778, <https://doi.org/10.1021/acs.est.1c05191>, 2022.
- Xu, Z. N., Nie, W., Liu, Y. L., Sun, P., Huang, D. D., Yan, C., Krechmer, J., Ye, P. L., Xu, Z., Qi, X. M., Zhu, C. J., Li, Y. Y., Wang, T. Y., Wang, L., Huang, X., Tang, R. Z., Guo, S., Xiu, G. L., Fu, Q. Y., Worsnop, D., Chi, X. G., and Ding, A. J.: Multifunctional Products of Isoprene Oxidation in Polluted Atmosphere and Their Contribution to SOA, *Geophys. Res. Lett.*, 48, e2020GL089276, <https://doi.org/10.1029/2020GL089276>, 2021.
- Zha, Q., Yan, C., Junninen, H., Riva, M., Sarnela, N., Aalto, J., Quéléver, L., Schallhart, S., Dada, L., Heikkinen, L., Peräkylä, O., Zou, J., Rose, C., Wang, Y., Mammarella, I., Katul, G., Vesala, T., Worsnop, D. R., Kulmala, M., Petäjä, T., Bianchi, F., and Ehn, M.: Vertical characterization of highly oxygenated molecules (HOMs) below and above a boreal forest canopy, *Atmos. Chem. Phys.*, 18, 17437–17450, <https://doi.org/10.5194/acp-18-17437-2018>, 2018.
- Zhang, Y., Li, D., Ma, Y., Dubois, C., Wang, X., Perrier, S., Chen, H., Wang, H., Jing, S., Lu, Y., Lou, S., Yan, C., Nie, W., Chen, J., Huang, C., George, C., and Riva, M.: Field Detection of Highly Oxygenated Organic Molecules in Shanghai by Chemical Ionization–Orbitrap, *Environ. Sci. Technol.*, 56, 7608–7617, <https://doi.org/10.1021/acs.est.1c08346>, 2022.
- Zhao, D., Pullinen, I., Fuchs, H., Schrade, S., Wu, R., Acir, I.-H., Tillmann, R., Rohrer, F., Wildt, J., Guo, Y., Kiendler-Scharr, A., Wahner, A., Kang, S., Vereecken, L., and Mentel, T. F.: Highly oxygenated organic molecule (HOM) formation in the isoprene oxidation by NO<sub>3</sub> radical, *Atmos. Chem. Phys.*, 21, 9681–9704, <https://doi.org/10.5194/acp-21-9681-2021>, 2021.